Robust T cell activation requires an eIF3-driven burst in T cell receptor translation

Authors: Dasmanthie De Silva[1,2], Lucas Ferguson[1], Grant H. Chin[1], Benjamin E. Smith[3], Ryan A. Apathy[4], Theodore L. Roth[4], Franziska Blaeschke[5], Marek Kudla[1], Alexander Marson[4,5,6,7,8,9,10], Nicholas T. Ingolia[1,11], Jamie H. D. Cate[1,2,10,11,12,13]*.

Affiliations:

[1]Department of Molecular and Cell Biology, University of California-Berkeley, Berkeley, California 94720, USA.

[2]The J. David Gladstone Institutes, San Francisco, CA 94158 USA.

[3]School of Optometry, University of California, Berkeley, Berkeley, CA 94720, USA.

[4]Department of Microbiology and Immunology, University of California, San Francisco, San Francisco, CA, USA.

[5]Gladstone-UCSF Institute of Genomic Immunology, San Francisco, CA 94158 USA.

[6]Diabetes Center, University of California, San Francisco, San Francisco, CA, USA.

[7]Chan Zuckerberg Biohub, San Francisco, CA, USA.

[8]Department of Medicine, University of California, San Francisco, San Francisco, CA, USA.

[9]Parker Institute for Cancer Immunotherapy, San Francisco, CA, USA.

20 [10]Innovative Genomics Institute, University of California, Berkeley, Berkeley, CA, USA.

21 [11]California Institute for Quantitative Biosciences, University of California, Berkeley,

22 Berkeley, USA.

23 [12]Department of Chemistry, University of California-Berkeley, Berkeley, California

24 94720, USA.

25 [13]Molecular Biophysics and Integrated Bioimaging Division, Lawrence Berkeley National

26 Laboratory, Berkeley, California 94720, USA.

27

28 *Correspondence to: j-h-doudna-cate@berkeley.edu.

29

ABSTRACT

Activation of T cells requires a rapid surge in cellular protein synthesis. However, the role of translation initiation in the early induction of specific genes remains unclear. Here we show human translation initiation factor eIF3 interacts with select immune system related mRNAs including those encoding the T cell receptor (TCR) subunits TCRA and TCRB. Binding of eIF3 to the *TCRA* and *TCRB* mRNA 3'-untranslated regions (3'-UTRs) depends on CD28 coreceptor signaling and regulates a burst in TCR translation required for robust T cell activation. Use of the *TCRA* or *TCRB* 3'-UTRs to control expression of an anti-CD19 chimeric antigen receptor (CAR) improves the ability of CAR-T cells to kill tumor cells *in vitro*. These results identify a new mechanism of eIF3-mediated translation control that can aid T cell engineering for immunotherapy applications.

KEYWORDS

eIF3, protein synthesis, 3'-untranslated region, T cell receptor, CD28, chimeric antigen receptor, cellular immunotherapy

53

54

55

56

57

58

59

60

61

62

63

64

65 **INTRODUCTION**

66 Translation initiation serves as a key gatekeeper of protein synthesis in eukaryotes
67 and requires the action of eukaryotic initiation factor 3 (eIF3) (Hernández et al., 2020;
68 Pelletier and Sonenberg, 2019). In humans, eIF3 is a 13-subunit protein complex that
69 coordinates the cellular machinery in positioning ribosomes at the mRNA start codon.
70 Several lines of evidence indicate eIF3 also serves specialized roles in cellular translation,
71 by recognizing specific RNA structures in the 5'-untranslated regions (5'-UTRs) of target
72 mRNAs (Lee et al., 2015), binding the 7-methyl-guanosine (m^7G) cap (Lamper et al.,
73 2020; Lee et al., 2016) or through interactions with *N*-6-methyl-adenosine (m^6A) post-
74 transcriptional modifications in mRNAs (Meyer et al., 2015). Binding to these *cis*-
75 regulatory elements in mRNA can lead to translation activation or repression, depending
76 on the RNA sequence and structural context (Lee et al., 2016, 2015; Meyer et al., 2015;
77 de la Parra et al., 2018). These noncanonical functions for eIF3 can aid cell proliferation
78 (Lee et al., 2015), or allow cells to rapidly adapt to stresses such as heat shock (Meyer
79 et al., 2015). T cell activation requires a rapid increase in protein synthesis within the first
80 few hours that also involves eIF3 (Ahern et al., 1974; Kleijn and Proud, 2002; Miyamoto
81 et al., 2005; Ricciardi et al., 2018). However, whether eIF3 serves a general or more
82 specific role in T cell activation is unknown.

83 Translation in non-activated lymphocytes is limited by the availability of translation
84 initiation factors (Ahern et al., 1974; Mao et al., 1992; Wolf et al., 2020). The mRNAs for
85 several translation initiation factors, including those for many eIF3 subunits, are repressed
86 in resting T cells and are rapidly translated within hours of activation (Wolf et al., 2020).
87 Additionally, nearly-inactive eIF3 in quiescent T cells is activated to form translation

88 initiation complexes in the first few hours after stimulation (Miyamoto et al., 2005).
89 Activation of eIF3 coincides with the recruitment of subunit eIF3j to eIF3 and translation
90 initiation complexes (Miyamoto et al., 2005). Post-translational modifications are also
91 thought to contribute to the early increase in translation, for example activation of the
92 guanine nucleotide exchange factor eIF2B (Kleijn and Proud, 2002). By contrast, the level
93 of the canonical mRNA cap-binding complex eIF4F–composed of translation initiation
94 factors eIF4E, eIF4G and eIF4A– increases much later after T cell activation (Mao et al.,
95 1992).

96 Recent studies have identified translational control of specific transcripts required
97 for the rewiring of metabolism needed for effector T cell function. Translation of these
98 specific transcripts involved in glycolysis and fatty acid synthesis occurs within 1-3 days
99 of T cell activation (Ricciardi et al., 2018), and depends on the activity of eIF4F. Hundreds
100 of other mRNAs translationally repressed in resting T cells are rapidly translated within
101 hours after activation, including those encoding key transcription factors and ribosomal
102 proteins, in addition to the translation initiation factors noted above (Wolf et al., 2020).
103 Most of these mRNAs are sensitive to mTOR inhibition, highlighting the importance of
104 eIF4F for the translation of these specific transcripts. However, a small subset of mRNAs
105 evade mTOR inhibition by an unknown mechanism (Wolf et al., 2020). Whether eIF3
106 selectively regulates these or other mRNAs early in T cell activation is not known.

107 In the adaptive immune system, T cells are activated when a foreign antigen is
108 recognized by the T cell receptor (TCR). However, robust T cell activation requires a
109 second signal generated by interactions between the T cell and antigen presenting cell
110 mediated by the co-receptor CD28 (Esensten et al., 2016). This two-signal mechanism

111 enables T cells to adopt a fully active state and avoid becoming unresponsive (Chen and
112 Flies, 2013). The process of T cell activation can be mimicked *in vitro* using antibodies
113 targeting both the TCR and CD28 (anti-CD3 and anti-CD28 antibodies, respectively)
114 (Harding et al., 1992), which has greatly aided the dissection of molecular mechanisms
115 underlying T cell activation.

116 Insights from these studies have also inspired efforts to engineer T cells for
117 immunotherapy applications such as treating cancers (Chen and Flies, 2013). T cells can
118 be engineered to express chimeric antigen receptors (CARs) that specifically target
119 antigens on the surface of cancer cells, and signal through protein elements derived from
120 both the TCR and CD28 or other co-stimulatory receptors (Chen and Flies, 2013;
121 Globerson Levin et al., 2021). The most successful of these CAR T cells have been used
122 to treat CD19-positive B cell malignancies, with dramatic results (Friedman et al., 2018;
123 Kalos et al., 2011; Kochenderfer et al., 2013; Qin et al., 2020; Wang et al., 2020).
124 However, CAR T cells still have a number of drawbacks, including toxicity, CAR T cell
125 exhaustion, limited persistence and poor efficacy in solid tumors. These problems
126 highlight the need for a deeper understanding of T cell activation and how it can be
127 controlled in CAR T cells (Globerson Levin et al., 2021; Watanabe et al., 2018).

128 Here, we identified mRNAs that specifically bind eIF3 in activated T cells, including
129 many encoding proteins involved in immune cell function such as the TCR. We mapped
130 the eIF3-dependent *cis*-regulatory elements in the mRNAs encoding the TCR alpha and
131 beta subunits (TCRA and TCRB, respectively), finding the 3'-untranslated regions (3'-
132 UTRs) of these mRNAs control a rapid burst in TCRA and TCRB translation that depends
133 on CD28 coreceptor signaling. Finally, we use this information to engineer T cells

134 expressing chimeric antigen receptors to modulate the dynamics of CAR expression and
135 improve the ability of CAR T cells to kill tumor cells *in vitro*.

136

137 **RESULTS**

138 **A specific suite of RNAs interact with eIF3 in activated Jurkat cells**

139 To delineate how eIF3 contributes to T cell activation, we first identified RNAs that
140 directly interact with eIF3 in Jurkat cells activated for 5 hours with phorbol 12-myristate
141 13-acetate and ionomycin (PMA+I), using photoactivatable ribonucleoside-enhanced
142 crosslinking and immunoprecipitation (PAR-CLIP) (Hafner et al., 2010; Lee et al., 2015;
143 Mukherjee et al., 2019) (**Figure 1A**). In the Jurkat PAR-CLIP experiments, RNA
144 crosslinked to eight of the thirteen eIF3 subunits, as identified by mass spectrometry:
145 subunits EIF3A, EIF3B, EIF3D and EIF3G as previously seen in HEK293T cells (Lee et
146 al., 2015), as well as subunits EIF3C, EIF3E, EIF3F, and EIF3L (**Figure 1B, Figure 1–**
147 **figure supplement 1A-1B, Supplementary File 1**). Consistent with its role in T cell
148 activation, eIF3 crosslinked to a substantially larger number of mRNAs (~75x more) in
149 activated Jurkat cells compared to control non-activated cells (**Figure1–figure**
150 **supplement 1C-1D and Supplementary Files 2 and 3**). Notably, in activated Jurkat cells
151 eIF3 interacted with mRNAs enriched for those encoding proteins central to immune cell
152 function, in contrast to those previously identified in HEK293T cells (Lee et al., 2015)
153 (**Figure 1C and Figure 1–figure supplement 1E**). The extent of eIF3 crosslinking in
154 activated Jurkat cells does not correlate with mRNA abundance (**Figure 1–figure**
155 **supplement 1F and Supplementary File 4**), suggesting the enrichment of immune

156 system related mRNAs reflects the involvement of eIF3 in specific regulation of T cell
157 activation.

158 In activated Jurkat cells, eIF3 showed a multitude of crosslinking patterns on
159 different mRNAs (**Figure 1D-1E and Figure 1–figure supplement 1D, 1G and 1H**),
160 consistent with varied roles for eIF3 in T cell activation and function. Many of the mRNAs
161 have a single PAR-CLIP site in the 5'-UTR as observed in HEK293T cells (Lee et al.,
162 2015) (**Figure 1D, Figure 1–figure supplement 1D, Supplementary File 3**). However,
163 eIF3 crosslinked to some mRNAs across the entire length of the transcript, from the
164 beginning of the 5'-UTR through the 3'-UTR (**Figure 1E and Figure 1–figure**
165 **supplement 1H**). This "pan-mRNA" pattern of eIF3 crosslinking–which includes
166 polyadenylated mRNAs as well as histone mRNAs–has not been observed before.
167 Interestingly, a number of these mRNAs encode proteins important for T cell activation,
168 including both the alpha and beta subunits of the T cell receptor (TCR), subunits TCRA
169 and TCRB (**Figure 1E, Supplementary File 5**).

170

171 ***TCRA* and *TCRB* mRNAs form distinct puncta in activated Jurkat cells**

172 Crosslinking in PAR-CLIP experiments requires direct interaction between the
173 RNA and protein of interest (Ascano et al., 2012). Thus, the pan-mRNA pattern of
174 crosslinking between eIF3 and certain mRNAs suggests formation of ribonucleoprotein
175 complexes (RNPs) highly enriched in eIF3. Notably, the pan-mRNA crosslinking pattern
176 in the *TCRA* and *TCRB* mRNAs occurs in activated but not in non-activated Jurkat cells
177 (**Figure 1E**), suggesting eIF3 may contribute to increased translation of these mRNAs
178 rather than their repression. We therefore examined *TCRA* and *TCRB* mRNA localization

179 in activated Jurkat cells, to determine whether they colocalized with repressive
180 environments such as P bodies or stress granules (Tauber et al., 2020). Since Jurkat cells
181 have a defined TCR, we designed fluorescence in situ hybridization (FISH) probes across
182 the entire *TCRA* and *TCRB* transcripts to examine their localization. Interestingly, the
183 *TCRA* and *TCRB* mRNAs formed distinct puncta in Jurkat cells activated with anti-
184 CD3/anti-CD28 antibodies, which induce both TCR and CD28 coreceptor signaling
185 required for robust T cell activation (Harding et al., 1992). However, these mRNAs did not
186 co-localize with either P bodies or stress granules, or with each other (**Figure 1F, Figure**
187 **1–figure supplement 2A and 2B**). These results indicate that the *TCRA* and *TCRB*
188 mRNAs are not translationally repressed but are likely localized to translation "hot spots."

189

190 **Pan-mRNAs remain bound to eIF3 in translating ribosomes**

191 The pan-mRNA crosslinking pattern suggests that eIF3 remains bound to the
192 *TCRA* and *TCRB* mRNAs while they are actively translated. To capture *TCRA* and *TCRB*
193 mRNAs in translating ribosomes and examine their interactions with eIF3, we analyzed
194 polysomes in Jurkat cells activated with anti-CD3/anti-CD28 antibodies (**Figure 2A**)
195 (Harding et al., 1992). The cells were first treated with protein-protein crosslinker
196 dithiobis(succinimidyl propionate) (DSP) before isolating polysomes on sucrose gradients
197 (**Figure 2–figure supplement 1A**). We then incubated the cell lysates with RNase H and
198 DNA oligonucleotides designed to cleave the mRNAs specifically between the 5'-UTR,
199 coding sequence (CDS), and 3'-UTR (**Figure 2B, Supplementary File 6**). This protocol
200 efficiently cleaved the mRNAs and prevented the released 5'-UTR and 3'-UTR elements
201 from entering polysomes (**Figure2–figure supplement 1B-1E**). It also allowed us to

202 detect eIF3 interactions with the mRNA CDS regions independent of eIF3 interactions
203 with the UTR sequences identified in the PAR-CLIP analysis. We detected mRNAs
204 interacting with eIF3 in the polysomes by performing anti-EIF3B immunoprecipitations
205 followed by qRT-PCR (**Figure 2A**). We compared both *TCRA* and *TCRB* mRNAs to
206 another pan-crosslinked mRNA, *DUSP2*, and to two mRNAs that crosslinked to eIF3 only
207 through their 5'-UTRs (*EGR1*, *TRIM28*). Using primers to the CDS regions of the mRNAs,
208 we found that eIF3 only immunoprecipitated the pan-crosslinked mRNAs (*TCRA*, *TCRB*,
209 *DUSP2*) from polysomes, but not mRNAs that only crosslinked to eIF3 through their 5'-
210 UTRs (*EGR1*, *TRIM28*) (**Figure 2C and 2D**). Importantly, all of these mRNAs are present
211 in translating ribosomes and can be immunoprecipitated with eIF3 when the mRNAs are
212 left intact (RNase H treatment without DNA oligos) (**Figure 2E**).

213 We also tested whether these mRNAs interact with eIF3 similarly in primary human
214 T cells during activation. We could not examine *TCRA* and *TCRB* mRNAs in primary
215 human T cells, as these mRNAs do not have a unique sequence in the 5'-UTR or variable
216 region of the CDS to which we could design DNA oligonucleotides as described above.
217 Therefore, we tested the distribution of *DUSP2*, *EGR1* and *TRIM28* mRNAs in primary
218 human T cells activated with anti-CD3/anti-CD28 antibodies (Harding et al., 1992). As
219 observed in Jurkat cells, *DUSP2* mRNA remained bound to eIF3 through its CDS region
220 in polysomes whereas the *EGR1* and *TRIM28* mRNAs did not remain bound (**Figure 2F–**
221 **2H**). We also confirmed that the 5'-UTR and 3'-UTR elements of these mRNAs are
222 efficiently cleaved and did not enter polysomes (**Figure2–figure supplement 1F–1H**).
223 Taken together, these results indicate that, in activated T cells, eIF3 remains bound to
224 the coding sequences (CDS) of the pan-mRNAs *TCRA*, *TCRB* and *DUSP2* in polysomes

225 independent of their 5'-UTR and 3'-UTR elements. These results further support the
226 model that *TCRA* and *TCRB* mRNA puncta represent translation "hot spots," and the pan-
227 mRNA crosslinking pattern reflects eIF3 binding to these mRNAs during translation
228 elongation.

229

230 **eIF3 interacts with the *TCRA* and *TCRB* mRNA 3'-UTRs and controls a burst in**
231 **translation during T cell activation**

232 Although crosslinking of eIF3 to the CDS regions of the *TCRA* and *TCRB* mRNAs
233 (**Figure 1E**) indicates eIF3 remains bound to them during translation elongation (**Figure**
234 **2 and Figure 2–figure supplement 1**), we wondered whether the 5'-UTRs and 3'-UTRs
235 might play a role in recruiting these mRNAs to translating ribosomes. The *TCRA* and
236 *TCRB* genes encode a different, often short 5'-UTR for each variable region of the mature
237 locus (Omer et al., 2021; Scaviner and Lefranc, 2000), suggesting the 5'-UTR is unlikely
238 to harbor eIF3-dependent regulatory elements. We therefore focused on the roles of the
239 *TCRA* and *TCRB* 3'-UTRs. We constructed nanoluciferase reporters fused to the WT
240 *TCRA* or *TCRB* mRNA 3'-UTR sequence, to 3'-UTRs with the eIF3 PAR-CLIP site deleted
241 (*ΔPAR*) or to 3'-UTRs with the reversed sequence of the eIF3 PAR-CLIP site (R**PAR*,
242 i.e. 5'-3' sequence reversed to 3'-5' direction to maintain the length of the 3'-UTR) (**Figure**
243 **3A**). We then stably expressed these mRNAs in primary human T cells using lentiviral
244 transduction and activated these T cells using anti-CD3/anti-CD28 antibodies. T cells
245 expressing the reporters with the WT *TCRA* or *TCRB* mRNA 3'-UTR sequences produced
246 substantially higher luminescence that peaked 1 hour after activation, while cells
247 expressing nanoluciferase from reporters with a deletion or reversal of the eIF3 PAR-

248 CLIP site sequence showed no apparent burst in translation (**Figure 3B**). The *TCRA*
249 Δ*PAR* or R**PAR* or *TCRB* Δ*PAR* or R**PAR* mutations, however, did not cause significant
250 defects in the nanoluciferase mRNA levels when compared to reporters with the
251 corresponding WT 3'-UTR sequences (**Figure 3C**)**.** This suggests the burst in
252 nanoluciferase expression observed with the WT *TCRA* or *TCRB* mRNA 3'-UTR
253 sequences is regulated posttranscriptionally. Immunoprecipitation of eIF3 followed by
254 qRT-PCR quantification of nanoluciferase mRNA showed that less nanoluciferase mRNA
255 bound to eIF3 when the 3'-UTR PAR-CLIP site was either deleted or reversed, compared
256 to nanoluciferase mRNAs carrying the WT *TCRA* or *TCRB* 3'-UTR (**Figure 3D and 3E**).
257 Interestingly, although the *TCRA* and *TCRB* mRNA 3'-UTR elements that crosslinked to
258 eIF3 do not share any conserved sequences or RNA structural elements (Xu and
259 Mathews, 2016), the above results support the idea that eIF3 binding to specific
260 sequences or structures within the *TCRA* and *TCRB* 3'-UTRs controls a burst in
261 translation after T cell activation.

262 We next tested whether the *TCRA* and *TCRB* 3'-UTRs serve to initially recruit eIF3
263 to the *TCRA* and *TCRB* mRNAs, as eIF3 does not remain stably bound to these 3'-UTRs
264 in translating ribosomes (**Figure 1–figure supplement 2G**). We made nanoluciferase
265 reporters in which we replaced the eIF3 PAR-CLIP site in the *TCRA* 3'-UTR with
266 sequences from the hepatitis C viral internal ribosome entry site (HCV IRES domain
267 IIIabc) or the *JUN* mRNA 5'-UTR, each previously shown to bind directly to eIF3 (Kieft et
268 al., 2001; Lee et al., 2015) (**Figure 3F**). We stably transduced these constructs into
269 primary T cells and measured nanoluciferase activity after activating the cells with anti-
270 CD3/anti-CD28 antibodies. By contrast to the *TCRA* Δ*PAR* 3'-UTR, the HCV IRES IIIabc

271 and *JUN* sequences increased nanoluciferase translation (**Figure 3G**). This was true
272 despite the fact that there was less of an increase in mRNA abundance for the HCV IRES
273 IIIabc and *JUN* constructs compared to the *TCRA* Δ*PAR* 3'-UTR (**Figure 3H**). The HCV
274 IRES IIIabc and *JUN* sequences also rescued eIF3 binding to the reporter mRNAs
275 (**Figure 3I**) upon T cell activation. These results are consistent with the engineered 3'-
276 UTRs recruiting eIF3 to the mRNA. However, the dynamics of translation activation
277 induced by the 3'-UTRs harboring the HCV IRES or *JUN* sequences did not recapitulate
278 the effects of the WT *TCRA* 3'-UTR. Both engineered 3'-UTRs increased nanoluciferase
279 levels within 30 minutes of activation, in contrast to the WT *TCRA* 3'-UTR (**Figure 3G**).
280 Furthermore, neither engineered 3'-UTR led to a marked decrease of nanoluciferase
281 levels after the 1 hour peak in luminescence seen with the WT *TCRA* 3'-UTR (**Figure**
282 **3G**). Taken together, the nanoluciferase reporter experiments reveal the *TCRA* and
283 *TCRB* mRNA 3'-UTRs are necessary and sufficient to drive a burst in translation after T
284 cell activation. They also suggest these 3'-UTR elements recruit eIF3 to the *TCRA* and
285 *TCRB* mRNAs to drive a burst in translation of the TCR alpha and beta subunits.

286

287 **The *TCRA* and *TCRB* mRNA 3'-UTRs control a burst in translation in a CD28-**
288 **dependent manner**

289 Since T cell activation in some cases does not require the TCR (Siefken et al.,
290 1998), we also tested whether the burst in translation controlled by the *TCRA* and *TCRB*
291 mRNA 3'-UTRs could be induced by activation of either the TCR or CD28 individually
292 (**Figure 4**). We found anti-CD28 stimulation alone was sufficient to cause a transient burst
293 in translation in the nanoluciferase reporters with the WT *TCRA* or *TCRB* mRNA 3'-UTRs,

294 whereas anti-CD3 stimulation caused a continuous increase in reporter protein
295 expression (**Figure 4B–4D**). Interestingly, the burst in translation required the reporters
296 to be membrane tethered via a N-terminal transmembrane helix (from CD3zeta) that is
297 co-translationally inserted into the membrane (Call and Wucherpfennig, 2005) (**Figure**
298 **4A–4D and Figure 4–figure supplement 1A–1C**), consistent with the fact that CD28
299 signaling involves multiple membrane-associated events (Boomer and Green, 2010).
300 Moreover, the reporters with *TCRA* Δ*PAR* and *TCRB* Δ*PAR* 3'-UTRs failed to show a
301 burst in expression even when the reporter proteins were tethered to the membrane
302 (**Figure 4A–4D**), supporting the role for eIF3 in the translational burst. Taken together,
303 these results support the model that the CD28 costimulatory pathway drives an early burst
304 in TCR translation after T cell activation, mediated by eIF3 binding to the *TCRA* and *TCRB*
305 3'-UTRs.

306 We also tested the proximal signaling pathways downstream of CD28 required for
307 the dynamic regulation of reporter expression by using inhibitors of the kinases AKT (Choi
308 et al., 2016; Wu et al., 2020) and mTOR (Thoreen et al., 2009). In T cells expressing the
309 membrane-tethered nanoluciferase reporter mRNA with the WT *TCRA* 3'-UTR (**Figure**
310 **4A**), treatment with the mTOR inhibitor Torin 1 had no effect on the rapid increase in
311 reporter expression as seen with the DMSO control. However the burst in nanoluciferase
312 expression was blocked when AKT kinase activity was inhibited with AZD5363 (AZD)
313 (**Figure 4E–4F and Figure 4–figure supplement 1D-1E**). Altogether, these data indicate
314 that the transient burst in TCR expression likely requires specific interactions between
315 eIF3 and the *TCRA* and *TCRB* 3'-UTRs and also membrane-proximal CD28 signaling.
316 Furthermore, these results support a model in which T cell activation requires CD28

317 costimulation to elicit an initial positive signal involving AKT kinase activity, which is later
318 repressed by a negative feedback loop also mediated by CD28 signaling and cis-
319 regulatory elements in the *TCRA* and *TCRB* mRNA 3'-UTRs.

320

321 **eIF3 interactions with the *TCRA* and *TCRB* mRNA 3'-UTRs regulate a burst in TCR**
322 **translation important for T cell activation**

323 Given that the *TCRA* and *TCRB* mRNA 3'-UTRs are necessary and sufficient to
324 drive a burst in translation after T cell activation, we examined their effects on the
325 endogenous levels of the TCR. We analyzed the expression of TCR protein levels using
326 western blots probed with an anti-TCRA antibody, since the formation of an intact TCR is
327 required to stabilize both the TCRA and TCRB subunits (Koning et al., 1988; Ohashi et
328 al., 1985). As seen with the nanoluciferase reporters, TCRA levels rose and peaked
329 approximately one hour after T cell activation with anti-CD3/anti-CD28 antibodies (**Figure**
330 **5A**). Furthermore, the early burst in TCRA translation is dependent on CD28 but not on
331 TCR signaling (**Figure 5A**), also as observed with membrane-tethered reporters (**Figure**
332 **4**). To more directly assess the role of the *TCRA* and *TCRB* mRNA 3'-UTRs, we used
333 CRISPR-Cas9 genome editing to delete the eIF3 PAR-CLIP sites in either the *TCRA* or
334 *TCRB* mRNA 3'-UTRs in primary T cells from two healthy human donors (**Figure 5–figure**
335 **supplement 1A and Supplementary File 6**). PCR analysis showed successful deletion
336 of the eIF3 PAR-CLIP site in the *TCRA* 3'-UTR or in the *TCRB* 3'-UTR (*TCRA* Δ*PAR* or
337 *TCRB* Δ*PAR*, respectively) in 43% - 49% of the alleles (**Figure 5–figure supplement**
338 **1B**). A scrambled sgRNA (SC), which does not target any site in the human genome was
339 used as a control. We first measured the total endogenous TCRA protein levels by

340 western blot in *TCRA* or *TCRB* 3'-UTR edited cells versus control cells at different time
341 points after activating with anti-CD3/anti-CD28 antibodies (**Figure 5B**). The SC control
342 cells – which should behave as wild-type T cells – exhibited a substantial burst in TCRA
343 protein levels immediately after activation (~1 hr). By contrast, TCRA protein levels were
344 nearly absent or clearly reduced at early time points after activation in both *TCRA* Δ*PAR*
345 and *TCRB* Δ*PAR* cell populations (**Figure 5B**). Only at later time points did TCRA levels
346 in the *TCRA* Δ*PAR* and *TCRB* Δ*PAR* cell populations begin to increase. These results
347 share the same pattern of expression seen with the nanoluciferase reporters described
348 above (**Figure 3 and Figure 4**).

349 We next asked whether the burst in TCR expression driven by the *TCRA* and
350 *TCRB* 3'-UTRs affected downstream steps in T cell activation. During TCR-dependent T
351 cell activation, membrane proteins reorganize at the interface between the T cell and
352 antigen presenting cell (APC) to form an immunological synapse (Huppa and Davis,
353 2003). TCR cluster formation is a central aspect of immune synapse formation (Cochran
354 et al., 2001). Therefore we tested whether TCR cluster formation is affected by reduced
355 TCR protein levels in *TCRA* Δ*PAR* and *TCRB* Δ*PAR* T cells at early time points after
356 activation. We used the same cell populations as those used for the western blots above
357 (**Figure 5B**), to correlate the TCRA protein levels observed in the western blots with TCR
358 clustering. We performed immunofluorescence on SC, *TCRA ΔPAR* and *TCRB ΔPAR* T
359 cell populations using anti-TCRA and anti-TCRB antibodies to detect the TCR. Both
360 *TCRA* Δ*PAR* and *TCRB* Δ*PAR* cells had fewer cells forming TCR clusters, especially at
361 the early time point compared to SC control cells when activated with anti-CD3/anti-CD28
362 (**Figure 5C and Figure 5–figure supplement 1C**). Consistent with the TCRA expression

363 levels observed in western blots and the rate of TCR clustering (**Figure 5B and 5C**), both
364 *TCRA* Δ*PAR* and *TCRB* Δ*PAR* cells expressed lower amounts of cell surface TCR
365 compared to SC control cells or cells edited with a single gRNA when tested by flow
366 cytometric analysis after PMA+I activation (**Figure 5–figure supplement 1D and 1E**).

367 To test whether the defect in TCR clustering in the *TCRA* Δ*PAR* and *TCRB* Δ*PAR*
368 cell populations reflects a general deficiency in T cell activation, we measured the T cell
369 activation markers CD69 and CD25 (IL2RA) by flow cytometry (**Figure 5–figure**
370 **supplement 1F and Figure 5–figure supplement 2A and 2B**). Fewer cells in the *TCRA*
371 Δ*PAR* and *TCRB* Δ*PAR* CD8+ and CD4+ primary T cell populations expressed CD69 at
372 early time points after activation (5-8 hours) (**Figure 5–figure supplement 2C and 2D**)
373 and fewer expressed both CD69 and CD25 at later time points after activation, compared
374 to SC control cells (**Figure 5D–5E and Figure 5–figure supplement 2E and 2F**). We
375 also found the *TCRA* Δ*PAR* and *TCRB* Δ*PAR* T cell populations secreted lower amounts
376 of cytokines IL2 (**Figure 5F and Figure 5–figure supplement 2G)** and IFNγ (**Figure 5G**
377 **and Figure 5–figure supplement 2H**), compared to the SC control cells. Taken together,
378 the *TCRA* Δ*PAR* and *TCRB* Δ*PAR* primary T cell populations exhibited multiple early and
379 late T cell activation defects. These results support the model that after T cell activation,
380 eIF3 binding to the *TCRA* and *TCRB* mRNA 3'-UTRs drives an early burst in TCR
381 translation that is required for many subsequent steps in T cell activation.

382 To obtain additional mechanistic understanding of eIF3-mediated regulation of
383 TCR translation we generated clonal *TCRA* Δ*PAR* and *TCRB* Δ*PAR* Jurkat cells using
384 the CRISPR-Cas9 genome editing strategy developed for primary T cells (**Figure 5–**
385 **figure supplement 1A, Supplementary File 6**). We first measured total TCR levels

386 using western blots and an anti-TCRA antibody as described above (**Figure 5A**), at
387 different time points after activation with anti-CD3/anti-CD28 antibodies. WT Jurkat cells
388 showed a TCR translational burst that peaked 5-8 hours after activation (**Figure 5–figure**
389 **supplement 3A**). By contrast, both *TCRA* Δ*PAR* and *TCRB* Δ*PAR* Jurkat cell populations
390 expressed lower levels of the TCR proteins compared to WT cells, and failed to show a
391 burst in TCR expression at early time points after activation (**Figure 5–figure**
392 **supplement 3A**). Importantly, *TCRA* and *TCRB* mRNA levels were unaffected or even
393 increased in the *TCRA* Δ*PAR* and *TCRB* Δ*PAR* Jurkat cells (**Figure 5–figure**
394 **supplement 3B and 3C**), similar to our observations with nanoluciferase reporters in
395 primary T cells (**Figure 3C**). This is consistent with TCR expression levels being regulated
396 post-transcriptionally by eIF3 interactions with the *TCRA* or *TCRB* mRNA 3'-UTR
397 elements. We then tested whether deleting eIF3 binding sites in both *TCRA* and *TCRB*
398 mRNA 3'-UTRs affected their interaction with eIF3. In both *TCRA* Δ*PAR* and *TCRB* Δ*PAR*
399 cells, eIF3 bound to significantly lower amounts of the *TCRA* and *TCRB* mRNAs
400 compared to WT cells at both the 5 hour and 8 hour time points after anti-CD3/anti-CD28
401 activation (**Figure 5–figure supplement 3D and 3E**). This indicates deleting the eIF3
402 PAR-CLIP sites in the 3'-UTR disrupts eIF3 interactions with the *TCRA* and *TCRB*
403 mRNAs substantially. Together with the nanoluciferase reporter experiments in primary
404 T cells (**Figure 3**), these results support the model that eIF3 binding to the 3'-UTR
405 elements of the *TCRA* and *TCRB* mRNAs mediates the rapid burst in TCR translation
406 after T cell activation.

407 **The *TCRA* and *TCRB* mRNA 3'-UTRs enhance anti-CD19 CAR T cell function**

408 T cells engineered to express chimeric antigen receptors (CARs) for cancer
409 immunotherapy now in use clinically employ artificial 3'-UTRs in the CAR-encoding
410 mRNA, a woodchuck hepatitis viral posttranscriptional regulatory element (*WPRE*)
411 (Milone et al., 2009), or a retroviral 3'-long terminal repeat (*3'-LTR*) (Kochenderfer et al.,
412 2009). However, it is not known whether these 3'-UTR elements provide optimal CAR
413 expression or CAR T cell function. To test whether these 3'-UTRs induce a transient burst
414 in translation as observed with the WT *TCRA* or *TCRB* 3'-UTRs, we fused the *WPRE* and
415 *3'-LTR* 3'-UTR sequences to nanoluciferase reporters and expressed these in primary T
416 cells (**Figure 6A**). In contrast to the *TCRA* and *TCRB* 3'-UTRs (**Figure 3 and Figure 4**),
417 the *WPRE* and *3'-LTR* 3'-UTR elements failed to induce the early burst in nanoluciferase
418 expression (**Figure 6A**). These data suggest that fusing the *TCRA* or *TCRB* 3'-UTR
419 sequences to engineered CAR open reading frames could be used to obtain more
420 physiological expression dynamics seen for the endogenous TCR.

421 We therefore engineered primary human T cells to express an anti-CD19 CAR
422 currently in use clinically to treat B cell lymphomas (Kalos et al., 2011; Milone et al., 2009;
423 June et al., 2014). We used lentiviral transduction to express the anti-CD19 CAR from
424 mRNAs with either *WPRE*, *3'-LTR*, *TCRA* or *TCRB* 3'-UTRs to make anti-CD19 CAR T
425 cells (**Figure 6B and 6C**). We then stimulated these CAR T cells by incubating them with
426 CD19-expressing leukemia cells (NALM6) and measured the CAR expression by western
427 blot analysis at different time points. Interestingly, the *TCRA* and *TCRB* 3'-UTRs induced
428 a burst in anti-CD19 CAR protein levels within 5 hours of NALM6 cell addition, whereas
429 the *WPRE* and *3'-LTR* sequences delayed the burst in CAR expression to ~24 hrs (**Figure**
430 **6D**). In these CAR T cells, TCR expression also followed the burst in CAR expression,

431 and was dependent on the presence of the CAR in addition to the NALM6 cells (**Figure**
432 **6–figure supplement 1A**). Lastly, we tested whether the timing of CAR protein
433 expression correlates with the killing capacity of these CAR T cells. Using *in vitro*
434 cytotoxicity assays (**Figure 6E**), CAR T cells expressing the CAR using either the *TCRA*
435 or *TCRB* 3'-UTR showed more robust killing of two tumor cell lines compared to CARs
436 using either the *WPRE* or *3'-LTR* 3'-UTRs (**Figure 6F–6G and Figure 6–figure**
437 **supplement 1B and 1C**). This is consistent with the importance of an early burst of CAR
438 translation for optimal CAR T cell function. These results also support the idea that using
439 the native *TCRA* or *TCRB* 3'-UTRs for CAR expression can be used to improve CAR T
440 cell function.

441

442 **DISCUSSION**

443 The eIF3 PAR-CLIP experiment we present here provides a snapshot of eIF3-RNA
444 interactions that occur at the time TCR translation is most sensitive to eIF3 regulation (5
445 hours in Jurkat cells, **Figure 5–figure supplement 3A**). At this point in time, eIF3
446 crosslinks to multiple mRNAs encoding proteins involved in immune cell function
447 (**Supplemental Files 2 and 3**). Interestingly, the patterns of eIF3 crosslinking, which for
448 a number of mRNAs include interactions with the protein coding sequence and 3'-UTR
449 (**Figure 1 and Figure 1–figure supplement 1G and 1H**), suggest an active role for eIF3
450 in promoting translation of these mRNAs. In support of this model, the two examples of
451 pan-mRNAs we examined here (*TCRA* and *TCRB*) reside in puncta distinct from P bodies
452 and stress granules (**Figure 1F**) and bind to eIF3 via the mRNA coding sequence on
453 translating ribosomes (**Figure 2**). However, this eIF3-mediated translation activation is

454 transient, lasting only 1-2 hours in primary T cells (**Figure 5A**). Importantly, the *TCRA* and
455 *TCRB* mRNA 3'-UTR elements are necessary and sufficient to control this burst in
456 translation (**Figure 3**). Recent evidence suggests that eIF3 can remain associated with
457 translating ribosomes (Bohlen et al., 2020; Lin et al., 2019; Wagner et al., 2020), a
458 phenomenon that seems to be enhanced for the pan-mRNAs identified here. Additional
459 layers of translation regulation also contribute to T cell function (Tan et al., 2017),
460 particularly with respect to mTOR signaling (Miyamoto et al., 2005; Myers et al., 2019)
461 and carbon metabolism (Manfrini et al., 2017; Ricciardi et al., 2018). The present PAR-
462 CLIP experiments should help to elucidate additional roles for eIF3-mediated translation
463 regulation and to map the system-wide role of translation regulation in T cell activation.

464 Recent experiments indicate that T cells must cross a threshold of T cell receptor
465 signaling to commit to activation and proliferation (Au-Yeung et al., 2014, 2017), setting
466 up a "digital" response to antigen recognition (Allison et al., 2016; Au-Yeung et al., 2014,
467 2017; Richard et al., 2018). The response threshold involves integration of intensity and
468 duration of TCR signaling (Au-Yeung et al., 2014, 2017; Richard et al., 2018), and spans
469 a wide range of TCR antigen affinity (Allison et al., 2016; Au-Yeung et al., 2014, 2017;
470 Richard et al., 2018). Notably, T cell commitment to clonal expansion and differentiation
471 can occur within as little as 1 to 2 hours of TCR stimulation for effector CD4+ and naive
472 CD8+ T cells (Iezzi et al., 1998; van Stipdonk et al., 2001). Remarkably, this time period
473 spans the burst in TCR protein synthesis mediated by eIF3 interactions with the *TCRA*
474 and *TCRB* mRNA 3'-UTR elements (**Figure 5A**). Naive CD4+ T cells require a longer
475 duration of TCR signaling of ~20 hours (Iezzi et al., 1998; Schrum et al., 2005). Although
476 we were not able to distinguish levels of TCR translation in isolated CD8+ and CD4+ T

477 cells (**Figure 5**), subsequent events in T cell activation including CD69 and CD25
478 expression, and IL2 and IFNγ secretion, were equally affected in CD8+ and CD4+ cells
479 in which the *TCRA* or *TCRB* 3'-UTR PAR-CLIP sites were deleted (**Figure 5C–5F**). In an
480 immune response, CD28 engagement serves as the second signal required for T cell
481 activation (Harding and Allison, 1993; Harding et al., 1992) and affects the first minutes
482 of TCR-mediated signaling (Green et al., 1994, 2000; Michel et al., 2001; Shahinian et
483 al., 1993; Tuosto and Acuto, 1998). Here we show CD28-mediated signaling is also
484 needed for the burst of TCR translation on the hour timescale in primary T cells (Buckler
485 et al., 2006) (**Figure 4**). Taken together, our results indicate that eIF3 controls *TCRA* and
486 *TCRB* mRNA translation during the first critical hours after antigen recognition that leads
487 to subsequent T cell commitment to proliferation and differentiation (**Figure 5**). The
488 requirement for CD28 in PD-1 mediated inhibition of T cell activation (Hui et al., 2017;
489 Kamphorst et al., 2017) also suggests eIF3-mediated control of TCR expression may
490 affect PD-1 checkpoint blockade-based cancer immunotherapy (Jiang et al., 2019).

491 Cell immunotherapies targeting various cancers have made great strides, due to
492 the engineering of chimeric antigen receptors that couple antigen recognition to
493 intracellular signaling domains that activate cytotoxic T cells. However, CAR T cells often
494 fail to eradicate cancers due to loss of activity over time, e.g. T cell exhaustion (Globerson
495 Levin et al., 2021; Watanabe et al., 2018). Our results using nanoluciferase reporters
496 indicated that eIF3-responsive mRNA 3'-UTR elements could be used to improve
497 chimeric antigen receptor expression and CAR T cell responsiveness (Eyquem et al.,
498 2017; Globerson Levin et al., 2021; Watanabe et al., 2018). We used this information to
499 improve the ability of CAR T cells to kill tumor cells *in vitro*. With a clinically validated anti-

500 CD19 CAR, we found that using the *TCRA* or *TCRB* mRNA 3'-UTRs dramatically
501 shortened the lag time before the burst in CAR protein expression upon exposure to tumor
502 cells (**Figure 6D**). This short lag time correlated with improved tumor cell killing in
503 cytotoxicity assays (**Figure 6E and 6F**). The burst in CAR protein expression was still not
504 as rapid as that of the endogenous TCR in T cells stimulated by anti-CD3/anti-CD28
505 antibodies, however (**Figure 5A**). This could be due to multiple factors, including CAR
506 affinity for the CD19 antigen or the activity of the 4-1BB costimulatory domain used in the
507 present CAR (Kalos et al., 2011; Milone et al., 2009; June et al., 2014) instead of the CD28
508 signaling domain (Kochenderfer et al., 2009). It is also possible that the 3'-UTRs of the
509 endogenous TCR subunits, which were left intact in the present cytotoxicity assays, and
510 which responded to CAR signaling (**Figure 6–figure supplement 1A**), titrated cellular
511 factors required for even shorter response times. T cell engineering to knock out the
512 endogenous TCR or improved CAR design may shorten the lag before the burst in CAR
513 expression and further improve CAR T cell function. Taken together, our experiments
514 delineate the central role of eIF3 in T cell activation and highlight the importance of
515 understanding translation regulation in immune cells to open new avenues for
516 engineering improved cell therapies (**Figure 7**).

517

518

519

520

521

522 **References and Notes:**

523 Ahern, T., Sampson, J., and Kay, J.E. (1974). Initiation of protein synthesis during
524 lymphocyte stimulation. Nature *248*, 519–521.

525 Allison, K.A., Sajti, E., Collier, J.G., Gosselin, D., Troutman, T.D., Stone, E.L., Hedrick,
526 S.M., and Glass, C.K. (2016). Affinity and dose of TCR engagement yield proportional
527 enhancer and gene activity in CD4+ T cells. Elife *5*.

528 Ascano, M., Hafner, M., Cekan, P., Gerstberger, S., and Tuschl, T. (2012). Identification
529 of RNA-protein interaction networks using PAR-CLIP. Wiley Interdiscip. Rev. RNA *3*,
530 159–177.

531 Au-Yeung, B.B., Zikherman, J., Mueller, J.L., Ashouri, J.F., Matloubian, M., Cheng,
532 D.A., Chen, Y., Shokat, K.M., and Weiss, A. (2014). A sharp T-cell antigen receptor
533 signaling threshold for T-cell proliferation. Proc. Natl. Acad. Sci. U. S. A. *111*, E3679–
534 E3688.

535 Au-Yeung, B.B., Smith, G.A., Mueller, J.L., Heyn, C.S., Jaszczak, R.G., Weiss, A., and
536 Zikherman, J. (2017). IL-2 Modulates the TCR Signaling Threshold for CD8 but Not
537 CD4 T Cell Proliferation on a Single-Cell Level. J. Immunol. *198*, 2445–2456.

538 Bohlen, J., Fenzl, K., Kramer, G., Bukau, B., and Teleman, A.A. (2020). Selective 40S
539 Footprinting Reveals Cap-Tethered Ribosome Scanning in Human Cells. Mol. Cell *79*,
540 561–574.e5.

541 Boomer, J.S., and Green, J.M. (2010). An enigmatic tail of CD28 signaling. Cold Spring

542 Harb. Perspect. Biol. *2*, a002436.

543 Buckler, J.L., Walsh, P.T., Porrett, P.M., Choi, Y., and Turka, L.A. (2006). Cutting edge:
544 T cell requirement for CD28 costimulation is due to negative regulation of TCR signals
545 by PTEN. J. Immunol. *177*, 4262–4266.

546 Call, M.E., and Wucherpfennig, K.W. (2005). The T cell receptor: critical role of the
547 membrane environment in receptor assembly and function. Annu. Rev. Immunol. *23*,
548 101–125.

549 Chen, L., and Flies, D.B. (2013). Molecular mechanisms of T cell co-stimulation and co-
550 inhibition. Nat. Rev. Immunol. *13*, 227–242.

551 Choi, A.-R., Kim, J.-H., Woo, Y.H., Cheon, J.H., Kim, H.S., and Yoon, S. (2016). Co-
552 treatment of LY294002 or MK-2206 with AZD5363 Attenuates AZD5363-induced
553 Increase in the Level of Phosphorylated AKT. Anticancer Res. *36*, 5849–5858.

554 Cochran, J.R., Aivazian, D., Cameron, T.O., and Stern, L.J. (2001). Receptor clustering
555 and transmembrane signaling in T cells. Trends Biochem. Sci. *26*, 304–310.

556 Dong, D., Zheng, L., Lin, J., Zhang, B., Zhu, Y., Li, N., Xie, S., Wang, Y., Gao, N., and
557 Huang, Z. (2019). Structural basis of assembly of the human T cell receptor-CD3
558 complex. Nature *573*, 546–552.

559 Esensten, J.H., Helou, Y.A., Chopra, G., Weiss, A., and Bluestone, J.A. (2016). CD28
560 Costimulation: From Mechanism to Therapy. Immunity *44*, 973–988.

561 Eyquem, J., Mansilla-Soto, J., Giavridis, T., van der Stegen, S.J.C., Hamieh, M.,

562 Cunanan, K.M., Odak, A., Gönen, M., and Sadelain, M. (2017). Targeting a CAR to the
563 TRAC locus with CRISPR/Cas9 enhances tumour rejection. Nature *543*, 113–117.

564 Friedman, K.M., Garrett, T.E., Evans, J.W., Horton, H.M., Latimer, H.J., Seidel, S.L.,
565 Horvath, C.J., and Morgan, R.A. (2018). Effective Targeting of Multiple B-Cell
566 Maturation Antigen-Expressing Hematological Malignances by Anti-B-Cell Maturation
567 Antigen Chimeric Antigen Receptor T Cells. Hum. Gene Ther. *29*, 585–601.

568 Globerson Levin, A., Rivière, I., Eshhar, Z., and Sadelain, M. (2021). CAR T cells:
569 Building on the CD19 paradigm. Eur. J. Immunol.

570 Green, J.M., Noel, P.J., Sperling, A.I., Walunas, T.L., Gray, G.S., Bluestone, J.A., and
571 Thompson, C.B. (1994). Absence of B7-dependent responses in CD28-deficient mice.
572 Immunity *1*, 501–508.

573 Green, J.M., Karpitskiy, V., Kimzey, S.L., and Shaw, A.S. (2000). Coordinate regulation
574 of T cell activation by CD2 and CD28. J. Immunol. *164*, 3591–3595.

575 Hafner, M., Landthaler, M., Burger, L., Khorshid, M., Hausser, J., Berninger, P.,
576 Rothballer, A., Ascano, M., Jr, Jungkamp, A.-C., Munschauer, M., et al. (2010).
577 Transcriptome-wide identification of RNA-binding protein and microRNA target sites by
578 PAR-CLIP. Cell *141*, 129–141.

579 Harding, F.A., and Allison, J.P. (1993). CD28-B7 interactions allow the induction of
580 CD8+ cytotoxic T lymphocytes in the absence of exogenous help. J. Exp. Med. *177*,
581 1791–1796.

582 Harding, F.A., McArthur, J.G., Gross, J.A., Raulet, D.H., and Allison, J.P. (1992). CD28-
583 mediated signalling co-stimulates murine T cells and prevents induction of anergy in T-
584 cell clones. Nature *356*, 607–609.

585 Hernández, G., García, A., Sonenberg, N., and Lasko, P. (2020). Unorthodox
586 Mechanisms to Initiate Translation Open Novel Paths for Gene Expression. J. Mol. Biol.
587 *432*, 166702.

588 Hui, E., Cheung, J., Zhu, J., Su, X., Taylor, M.J., Wallweber, H.A., Sasmal, D.K., Huang,
589 J., Kim, J.M., Mellman, I., et al. (2017). T cell costimulatory receptor CD28 is a primary
590 target for PD-1-mediated inhibition. Science *355*, 1428–1433.

591 Huppa, J.B., and Davis, M.M. (2003). T-cell-antigen recognition and the immunological
592 synapse. Nat. Rev. Immunol. *3*, 973–983.

593 Iezzi, G., Karjalainen, K., and Lanzavecchia, A. (1998). The duration of antigenic
594 stimulation determines the fate of naive and effector T cells. Immunity *8*, 89–95.

595 Jiang, Y., Chen, M., Nie, H., and Yuan, Y. (2019). PD-1 and PD-L1 in cancer
596 immunotherapy: clinical implications and future considerations. Hum. Vaccin.
597 Immunother. *15*, 1111–1122.

598 June, C.H., Levine, B.L., Porter, D.L., Kalos, M.D., and Milone, M.C. (2014).
599 Compositions for treatment of cancer.

600 Kalos, M., Levine, B.L., Porter, D.L., Katz, S., Grupp, S.A., Bagg, A., and June, C.H.
601 (2011). T cells with chimeric antigen receptors have potent antitumor effects and can

602 establish memory in patients with advanced leukemia. Sci. Transl. Med. *3*, 95ra73.

603 Kamphorst, A.O., Wieland, A., Nasti, T., Yang, S., Zhang, R., Barber, D.L., Konieczny,
604 B.T., Daugherty, C.Z., Koenig, L., Yu, K., et al. (2017). Rescue of exhausted CD8 T
605 cells by PD-1-targeted therapies is CD28-dependent. Science *355*, 1423–1427.

606 Kieft, J.S., Zhou, K., Jubin, R., and Doudna, J.A. (2001). Mechanism of ribosome
607 recruitment by hepatitis C IRES RNA. RNA *7*, 194–206.

608 Kleijn, M., and Proud, C.G. (2002). The regulation of protein synthesis and translation
609 factors by CD3 and CD28 in human primary T lymphocytes. BMC Biochem. *3*, 11.

610 Kochenderfer, J.N., Feldman, S.A., Zhao, Y., Xu, H., Black, M.A., Morgan, R.A., Wilson,
611 W.H., and Rosenberg, S.A. (2009). Construction and preclinical evaluation of an anti-
612 CD19 chimeric antigen receptor. J. Immunother. *32*, 689–702.

613 Kochenderfer, J.N., Dudley, M.E., Carpenter, R.O., Kassim, S.H., Rose, J.J., Telford,
614 W.G., Hakim, F.T., Halverson, D.C., Fowler, D.H., Hardy, N.M., et al. (2013). Donor-
615 derived CD19-targeted T cells cause regression of malignancy persisting after
616 allogeneic hematopoietic stem cell transplantation. Blood *122*, 4129–4139.

617 Koning, F., Lew, A.M., Maloy, W.L., Valas, R., and Coligan, J.E. (1988). The
618 biosynthesis and assembly of T cell receptor alpha- and beta-chains with the CD3
619 complex. J. Immunol. *140*, 3126–3134.

620 Lamper, A.M., Fleming, R.H., Ladd, K.M., and Lee, A.S.Y. (2020). A phosphorylation-
621 regulated eIF3d translation switch mediates cellular adaptation to metabolic stress.

622 Science *370*, 853–856.

623 Lee, A.S., Kranzusch, P.J., Doudna, J.A., and Cate, J.H.D. (2016). eIF3d is an mRNA
624 cap-binding protein that is required for specialized translation initiation. Nature *536*, 96–
625 99.

626 Lee, A.S.Y., Kranzusch, P.J., and Cate, J.H.D. (2015). eIF3 targets cell-proliferation
627 messenger RNAs for translational activation or repression. Nature *522*, 111–114.

628 Lin, Y., Li, F., Huang, L., Duan, H., Fang, J., Sun, L., Xing, X., Tian, G., Cheng, Y.,
629 Yang, X., et al. (2019). eIF3 associates with 80S ribosomes to promote translation
630 elongation, mitochondrial homeostasis, and muscle health.

631 Manfrini, N., Ricciardi, S., Miluzio, A., Fedeli, M., Scagliola, A., Gallo, S., Brina, D.,
632 Adler, T., Busch, D.H., Gailus-Durner, V., et al. (2017). High levels of eukaryotic
633 Initiation Factor 6 (eIF6) are required for immune system homeostasis and for steering
634 the glycolytic flux of TCR-stimulated CD4+ T cells in both mice and humans. Dev.
635 Comp. Immunol. *77*, 69–76.

636 Mao, X., Green, J.M., Safer, B., Lindsten, T., Frederickson, R.M., Miyamoto, S.,
637 Sonenberg, N., and Thompson, C.B. (1992). Regulation of translation initiation factor
638 gene expression during human T cell activation. J. Biol. Chem. *267*, 20444–20450.

639 Meyer, K.D., Patil, D.P., Zhou, J., Zinoviev, A., Skabkin, M.A., Elemento, O., Pestova,
640 T.V., Qian, S.-B., and Jaffrey, S.R. (2015). 5’ UTR m(6)A Promotes Cap-Independent
641 Translation. Cell *163*, 999–1010.

642 Michel, F., Attal-Bonnefoy, G., Mangino, G., Mise-Omata, S., and Acuto, O. (2001).
643 CD28 as a molecular amplifier extending TCR ligation and signaling capabilities.
644 Immunity *15*, 935–945.

645 Milone, M.C., Fish, J.D., Carpenito, C., Carroll, R.G., Binder, G.K., Teachey, D.,
646 Samanta, M., Lakhal, M., Gloss, B., Danet-Desnoyers, G., et al. (2009). Chimeric
647 receptors containing CD137 signal transduction domains mediate enhanced survival of
648 T cells and increased antileukemic efficacy in vivo. Mol. Ther. *17*, 1453–1464.

649 Miyamoto, S., Patel, P., and Hershey, J.W.B. (2005). Changes in ribosomal binding
650 activity of eIF3 correlate with increased translation rates during activation of T
651 lymphocytes. J. Biol. Chem. *280*, 28251–28264.

652 Mukherjee, N., Wessels, H.-H., Lebedeva, S., Sajek, M., Ghanbari, M., Garzia, A.,
653 Munteanu, A., Yusuf, D., Farazi, T., Hoell, J.I., et al. (2019). Deciphering human
654 ribonucleoprotein regulatory networks. Nucleic Acids Res. *47*, 570–581.

655 Myers, D.R., Wheeler, B., and Roose, J.P. (2019). mTOR and other effector kinase
656 signals that impact T cell function and activity. Immunol. Rev. *291*, 134–153.

657 Ohashi, P.S., Mak, T.W., Van den Elsen, P., Yanagi, Y., Yoshikai, Y., Calman, A.F.,
658 Terhorst, C., Stobo, J.D., and Weiss, A. (1985). Reconstitution of an active surface
659 T3/T-cell antigen receptor by DNA transfer. Nature *316*, 606–609.

660 Omer, A., Peres, A., Rodriguez, O.L., Watson, C.T., Lees, W., Polak, P., Collins, A.M.,
661 and Yaari, G. (2021). T Cell Receptor Beta (TRB) Germline Variability is Revealed by
662 Inference From Repertoire Data.

663 Park, J.H., Rivière, I., Gonen, M., Wang, X., Sénéchal, B., Curran, K.J., Sauter, C.,
664 Wang, Y., Santomasso, B., Mead, E., et al. (2018). Long-Term Follow-up of CD19 CAR
665 Therapy in Acute Lymphoblastic Leukemia. N. Engl. J. Med. *378*, 449–459.

666 de la Parra, C., Ernlund, A., Alard, A., Ruggles, K., Ueberheide, B., and Schneider, R.J.
667 (2018). A widespread alternate form of cap-dependent mRNA translation initiation. Nat.
668 Commun. *9*, 3068.

669 Pelletier, J., and Sonenberg, N. (2019). The Organizing Principles of Eukaryotic
670 Ribosome Recruitment. Annu. Rev. Biochem. *88*, 307–335.

671 Qin, J.S., Johnstone, T.G., Baturevych, A., Hause, R.J., Ragan, S.P., Clouser, C.R.,
672 Jones, J.C., Ponce, R., Krejsa, C.M., Salmon, R.A., et al. (2020). Antitumor Potency of
673 an Anti-CD19 Chimeric Antigen Receptor T-Cell Therapy, Lisocabtagene Maraleucel in
674 Combination With Ibrutinib or Acalabrutinib. J. Immunother. *43*, 107–120.

675 Ricciardi, S., Manfrini, N., Alfieri, R., Calamita, P., Crosti, M.C., Gallo, S., Müller, R.,
676 Pagani, M., Abrignani, S., and Biffo, S. (2018). The Translational Machinery of Human
677 CD4+ T Cells Is Poised for Activation and Controls the Switch from Quiescence to
678 Metabolic Remodeling. Cell Metab. *28*, 895–906.e5.

679 Richard, A.C., Lun, A.T.L., Lau, W.W.Y., Göttgens, B., Marioni, J.C., and Griffiths, G.M.
680 (2018). T cell cytolytic capacity is independent of initial stimulation strength. Nat.
681 Immunol. *19*, 849–858.

682 Scaviner, D., and Lefranc, M.P. (2000). The human T cell receptor alpha variable
683 (TRAV) genes. Exp. Clin. Immunogenet. *17*, 83–96.

684 Schrum, A.G., Palmer, E., and Turka, L.A. (2005). Distinct temporal programming of
685 naive CD4+ T cells for cell division versus TCR-dependent death susceptibility by
686 antigen-presenting macrophages. Eur. J. Immunol. *35*, 449–459.

687 Shahinian, A., Pfeffer, K., Lee, K.P., Kündig, T.M., Kishihara, K., Wakeham, A., Kawai,
688 K., Ohashi, P.S., Thompson, C.B., and Mak, T.W. (1993). Differential T cell
689 costimulatory requirements in CD28-deficient mice. Science *261*, 609–612.

690 Siefken, R., Klein-Hessling, S., Serfling, E., Kurrle, R., and Schwinzer, R. (1998). A
691 CD28-associated signaling pathway leading to cytokine gene transcription and T cell
692 proliferation without TCR engagement. J. Immunol. *161*, 1645–1651.

693 van Stipdonk, M.J., Lemmens, E.E., and Schoenberger, S.P. (2001). Naïve CTLs
694 require a single brief period of antigenic stimulation for clonal expansion and
695 differentiation. Nat. Immunol. *2*, 423–429.

696 Tan, H., Yang, K., Li, Y., Shaw, T.I., Wang, Y., Blanco, D.B., Wang, X., Cho, J.-H.,
697 Wang, H., Rankin, S., et al. (2017). Integrative Proteomics and Phosphoproteomics
698 Profiling Reveals Dynamic Signaling Networks and Bioenergetics Pathways Underlying
699 T Cell Activation. Immunity *46*, 488–503.

700 Tauber, D., Tauber, G., and Parker, R. (2020). Mechanisms and Regulation of RNA
701 Condensation in RNP Granule Formation. Trends Biochem. Sci. *45*, 764–778.

702 Thoreen, C.C., Kang, S.A., Chang, J.W., Liu, Q., Zhang, J., Gao, Y., Reichling, L.J.,
703 Sim, T., Sabatini, D.M., and Gray, N.S. (2009). An ATP-competitive mammalian target
704 of rapamycin inhibitor reveals rapamycin-resistant functions of mTORC1. J. Biol. Chem.

705 *284*, 8023–8032.

706 Tuosto, L., and Acuto, O. (1998). CD28 affects the earliest signaling events generated
707 by TCR engagement. Eur. J. Immunol. *28*, 2131–2142.

708 Wagner, S., Herrmannová, A., Hronová, V., Gunišová, S., Sen, N.D., Hannan, R.D.,
709 Hinnebusch, A.G., Shirokikh, N.E., Preiss, T., and Valášek, L.S. (2020). Selective
710 Translation Complex Profiling Reveals Staged Initiation and Co-translational Assembly
711 of Initiation Factor Complexes. Mol. Cell *79*, 546–560.e7.

712 Wang, M., Munoz, J., Goy, A., Locke, F.L., Jacobson, C.A., Hill, B.T., Timmerman, J.M.,
713 Holmes, H., Jaglowski, S., Flinn, I.W., et al. (2020). KTE-X19 CAR T-Cell Therapy in
714 Relapsed or Refractory Mantle-Cell Lymphoma. N. Engl. J. Med. *382*, 1331–1342.

715 Watanabe, K., Kuramitsu, S., Posey, A.D., Jr, and June, C.H. (2018). Expanding the
716 Therapeutic Window for CAR T Cell Therapy in Solid Tumors: The Knowns and
717 Unknowns of CAR T Cell Biology. Front. Immunol. *9*, 2486.

718 Wolf, T., Jin, W., Zoppi, G., Vogel, I.A., Akhmedov, M., Bleck, C.K.E., Beltraminelli, T.,
719 Rieckmann, J.C., Ramirez, N.J., Benevento, M., et al. (2020). Dynamics in protein
720 translation sustaining T cell preparedness. Nat. Immunol. *21*, 927–937.

721 Wu, Y.-H., Huang, Y.-F., Chen, C.-C., Huang, C.-Y., and Chou, C.-Y. (2020).
722 Comparing PI3K/Akt Inhibitors Used in Ovarian Cancer Treatment. Front. Pharmacol.
723 *11*, 206.

724 Xu, Z.Z., and Mathews, D.H. (2016). Prediction of Secondary Structures Conserved in

725 Multiple RNA Sequences. Methods Mol. Biol. *1490*, 35–50.

726

727 **Acknowledgments:** We thank M. Hafner for advice on PAR-CLIP methodology and
728 data analysis, A. Weiss for experimental suggestions and advice, H. Nolla and A.
729 Valeros at the UC Berkeley flow cytometry facility for helping out with the FACS analysis
730 and single cell sorting, F. Ives and H. L. Aaron at the UC Berkeley Imaging center for
731 help with microscopy, J. Lui and J. Bohlen for advice on planning experiments and for
732 suggestions on the manuscript, N. Aleksashin and A.M. González-Sánchez for advice
733 on the manuscript, and M. Mignardi for advice on FISH experiments. Figure 6E and 7
734 were created using Biorender. com. **Funding:** This work was supported by NIH grant
735 R01-GM065050 (J.H.D.C.) and a grant from the Tang Prize for Biopharmaceutical
736 Science (J.H.D.C.). N.T.I. is a Damon Runyon-Rachleff Innovator (DRR#37-15) and NIH
737 New Innovator (DP2 CA195768). A.M. holds a Career Award for Medical Scientists from
738 the Burroughs Wellcome Fund and The Cancer Research Institute (CRI) Lloyd J. Old
739 STAR grant and has received funding from the Chan Zuckerberg Biohub, Innovative
740 Genomics Institute (IGI) and the Parker Institute for Cancer Immunotherapy (PICI).
741 B.E.S. is supported by NIH grant P30EY003176. Imaging experiments were conducted
742 at the Cancer Research Laboratory Molecular Imaging Center, supported by Helen Wills
743 Neuroscience Institute. Sequencing was carried out at the UCSF Center for Advanced
744 Technology and at the Vincent J. Coates Genomics Sequencing Laboratory at UC
745 Berkeley, supported by NIH grant S10 OD018174. F.B. was supported by the Care-for-
746 Rare Foundation and the German Research Foundation (DFG). **Author Contributions:**
747 Project and experiments were conceived and designed by D.D.S. and J.H.D.C. D.D.S.
748 carried out all experiments, with assistance from B.E.S. and G.H.C. for image
749 acquisition and analysis, from T.R., R.A.A., F.B. and A.M. for primary T cell genome

editing and cell culture protocols, and from L.F., M.K., N.T.I. and J.H.D.C. for analysis of deep sequencing-based experiments. The manuscript was written by D.D.S. and J.H.D.C., with editing by all authors. **Declaration of Interests:** The authors declare competing financial interests: T.L.R. and A.M. are co-founders of Arsenal Therapeutics. A.M. is a co-founder of Spotlight Therapeutics. A.M. served on the scientific advisory board of PACT Pharma, was an advisor to Juno Therapeutics and Trizell. The Marson Laboratory has received research support from Juno Therapeutics, Epinomics, Sanofi, GlaxoSmithKline,Gilead and Anthem. A provisional patent application has been filed on some of the work presented herein. **Data and Materials Availability:** Sequencing data supporting the findings in this study have been deposited in the Gene Expression Omnibus (GEO) Database (https://www.ncbi.nlm.nih.gov/geo/), with accession codes _____. Code used to analyze the microscopy images is available on github at https://github.com/Llamero/TCR_colocalization_analysis-macro.

Supplementary Materials:

Materials and Methods

Figure supplements

Captions for Supplemental Files 1-6

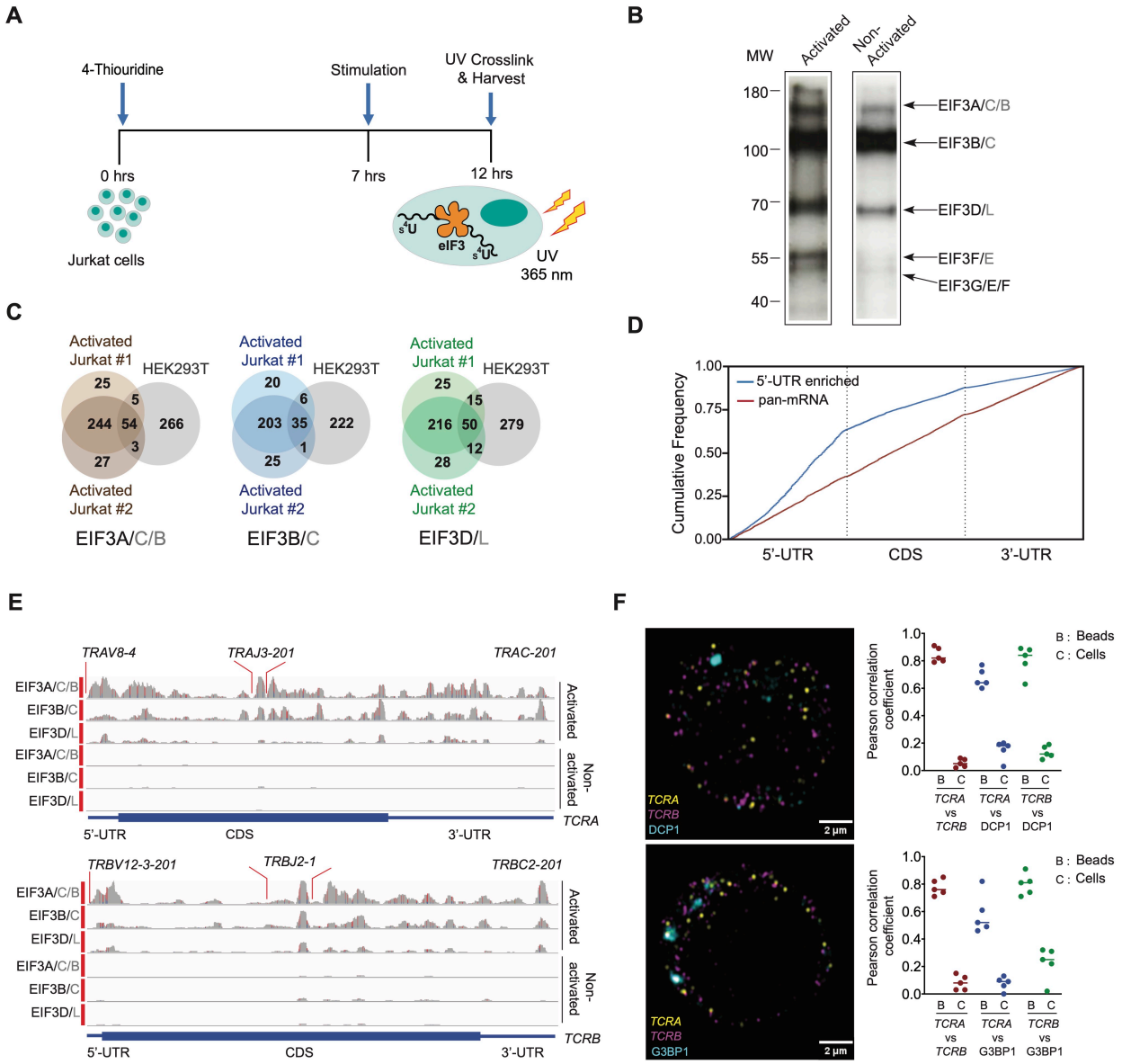

Figure 1. eIF3 interacts with specific mRNAs related to immune function in activated Jurkat cells. (**A**) Schematic of the PAR-CLIP experiment in Jurkat cells, showing steps through cell harvesting. (**B**) Phosphorimage of SDS polyacrylamide gel resolving 5′ ^{32}P-labeled RNAs crosslinked to eIF3 subunits in activated and non-activated Jurkat cells, from one of two biological replicates. (**C**) Venn diagram of genes identified by eIF3 PAR-CLIP in activated Jurkat cells from two biological replicates, compared with

774 the eIF3 PAR-CLIP mRNAs previously identified in HEK293T cells. The same number of
775 mRNAs from the Jurkat cell PAR-CLIP libraries, ranked by total reads mapped to a given
776 gene, are compared to the number of mRNAs identified in the HEK293T PAR-CLIP
777 experiments. (**D**) Varied mRNA crosslinking patterns to eIF3 in activated Jurkat cells.
778 Cumulative plot showing mRNA crosslinking in sample EIF3A/C/B to predominantly the
779 5'-UTR (n = 396, 414 mRNAs in replicates 1 and 2, respectively), and across the entire
780 length of some mRNAs ("pan-mRNAs", n = 634, 621 mRNAs). The 5'-UTR, CDS, and 3'-
781 UTR regions are shown normalized by length. (**E**) Crosslinking of the eIF3 subunits as
782 indicated across the entire *TCRA* and *TCRB* mRNAs, in activated and non-activated
783 Jurkat cells. 5'-UTR, coding sequence (CDS), and 3'-UTR elements (below) along with
784 the variable (V), joining (J) and constant (C) regions (above) for the mapped TCR genes
785 in Jurkat cells are shown. The blue and red vertical lines in the plotted reads indicate the
786 amount of T-C transitions vs other mutations, respectively for a particular nucleotide. The
787 *TCRA* and *TCRB* mRNAs are present in both non-activated and activated Jurkat cells
788 (**Supplementary File 4**). (**F**) FISH analysis of *TCRA* and *TCRB* mRNAs (yellow and
789 magenta, respectively) and P bodies (top) marked by the location of DCP1 (cyan) and
790 stress granules (bottom) marked by the location of G3BP1 (cyan), in activated Jurkat
791 cells. Graphs to the right of the images indicate Pearson's correlation coefficients (PCCs)
792 of *TCRA* and *TCRB* mRNAs localizing with each other or with P bodies or stress granules.
793 TetraSpeck™ microsphere beads were used as a positive control for colocalization.
794 Labels on the x axis are, B: TetraSpeck™ microsphere beads, C: activated Jurkat cells.
795 (n = 5, P <0.008, for PCC values of cells relative to bead colocalization, across all the

796 channels tested, using the Wilcoxon rank-sum test). Images are representative of one
797 experiment of the five independent experiments in the graphs.

798

799

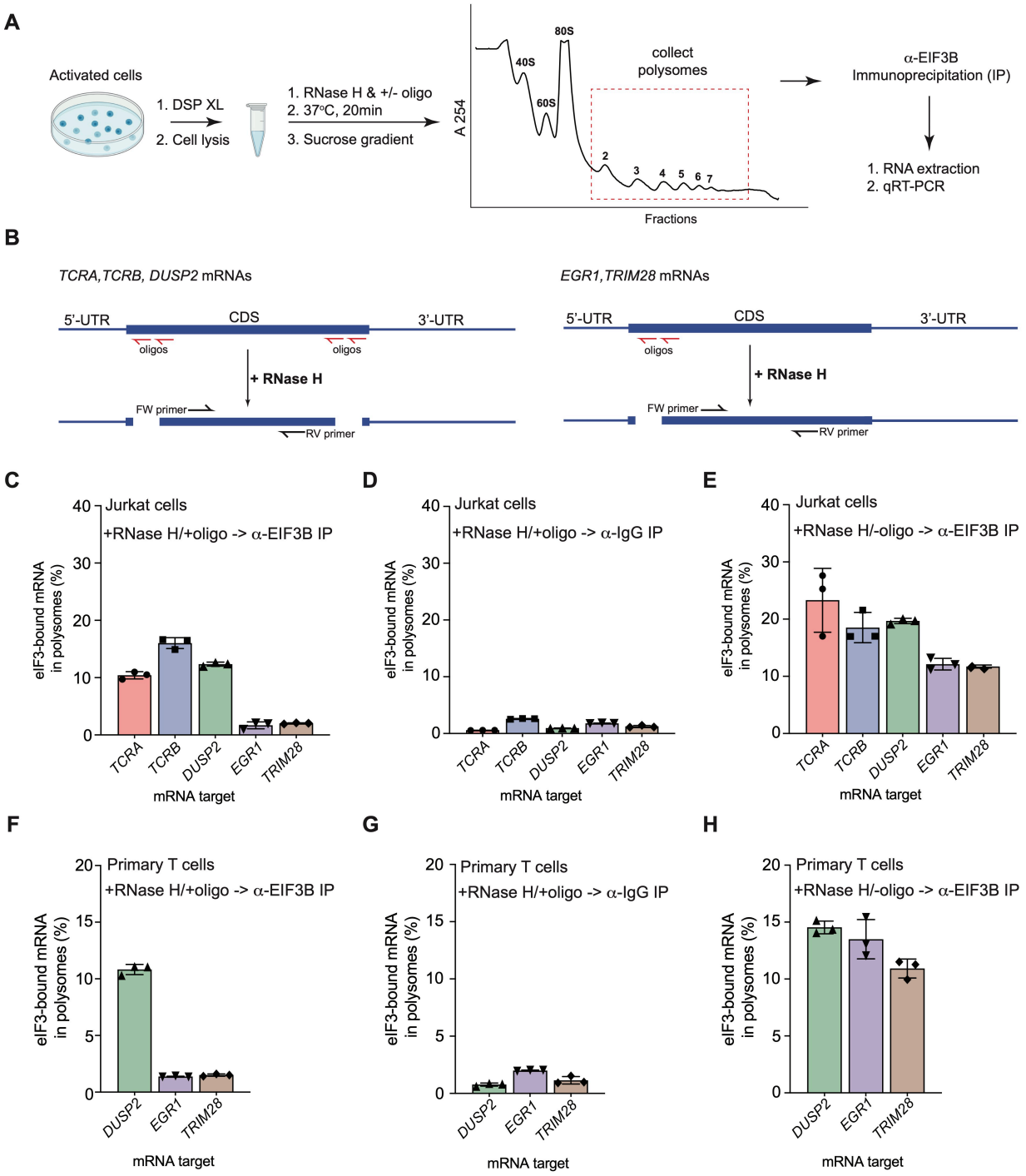

Figure 2. eIF3 remains bound to the coding sequences (CDS) of pan-mRNAs independent of their 5'-UTR and 3'-UTR elements in actively translating ribosomes. (**A**) Schematic outlining the RNase H-based assay of eIF3 interactions with mRNAs in

804 polysomes. DSP refers to the dithiobis (succinimidyl propionate) crosslinking agent.
805 Oligos, DNA oligos designed for RNase H-mediated targeting and cleavage of specific
806 mRNAs. (**B**) Strategy for detecting mRNA fragments released by RNase H digestion. Red
807 arrows denote DNA oligos for RNase H-mediated targeting of mRNAs. RT-qPCR primers
808 (black) were used to detect the CDS regions of the mRNAs. (**C**) Amount of eIF3-bound
809 mRNA co-immunoprecipitated by an anti-EIF3B antibody (Lee et al., 2015), from
810 polysome fractions of Jurkat cells treated with RNase H and oligos targeting the CDS-
811 UTR junctions (red arrows diagrammed in panel **B**). (**D**) Amount of eIF3-bound mRNA
812 co-immunoprecipitated with IgG beads, from polysome fractions of Jurkat cell lysate
813 treated with RNase H and oligos targeting the CDS-UTR junctions. (**E**) Amount of eIF3-
814 bound mRNA co-immunoprecipitated by the anti-EIF3B antibody, from polysome
815 fractions of Jurkat cell lysate treated only with RNase H. (**F**) Amount of eIF3-bound mRNA
816 co-immunoprecipitated by an anti-EIF3B antibody, from polysome fractions of primary
817 human T cells treated with RNase H and oligos targeting the CDS-UTR junctions (red
818 arrows diagrammed in panel **B**). (**G**) Amount of eIF3-bound mRNA co-
819 immunoprecipitated with IgG beads, from polysome fractions of primary human T cell
820 lysate treated with RNase H and oligos targeting the CDS-UTR junctions. (**H**) Amount of
821 eIF3-bound mRNA co-immunoprecipitated by the anti-EIF3B antibody, from polysome
822 fractions of primary human T cell lysate treated only with RNase H. In panels **C**–**H**, the
823 percentage is relative to the amount of total mRNA present in the polysome fraction prior
824 to immunoprecipitation. All the immunoprecipitation experiments in panels **C**–**H** were
825 carried out in biological duplicate with one technical triplicate shown (n = 3, with mean

826 and standard deviations shown). The primary human T cell experiment was done using

827 2 donors.

828

829

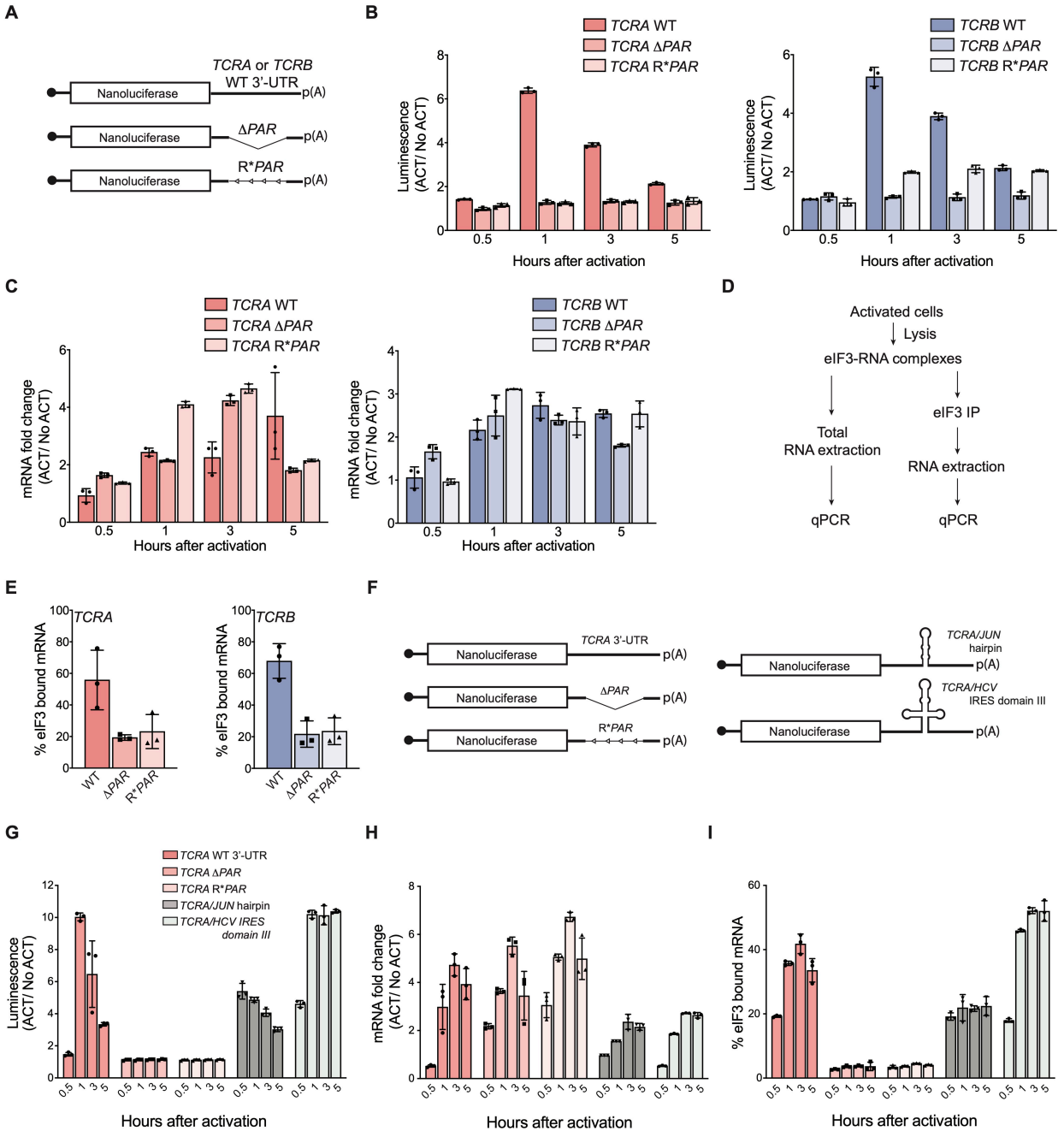

Figure 3. Interaction of eIF3 with *TCRA* and *TCRB* mRNA 3'-UTR elements mediates a burst in TCR translation in primary human T cells. (**A**) Schematic of nanoluciferase reporters stably expressed in primary human T cells. The reporters carry the *HBB* 5'-UTR and WT, *ΔPAR* or R**PAR* 3'-UTRs. WT, intact 3'-UTR from either *TCRA* or *TCRB* mRNA; *ΔPAR*, 3'-UTR of *TCRA* or *TCRB* with the eIF3 PAR-CLIP site deleted; R**PAR*, reversed

836 PAR-CLIP sequence in the 3'-UTR of *TCRA* or *TCRB* mRNA. (**B**) Luciferase activity in
837 anti-CD3/anti-CD28 activated T cells stably expressing nanoluciferase constructs
838 described in **A**, relative to non-activated controls (ACT/NoACT). (**C**) Changes in
839 nanoluciferase mRNA levels in **B**, as determined by qRT-PCR. (**D**) Schematic of
840 immunoprecipitation of eIF3 using an anti-EIF3B antibody (Lee et al., 2015), followed by
841 qRT-PCR to quantify the amount of nanoluciferase mRNA bound to eIF3. (**E**)
842 Immunoprecipitation as shown in **D** showing the amount of nanoluciferase mRNA bound
843 to eIF3 in T cells stably transduced with either *TCRA* (left) or *TCRB* (right) WT, *ΔPAR* or
844 R**PAR* 3'-UTRs after activation with anti-CD3/anti-CD28 antibodies for 1 hour. The
845 percent mRNA bound to anti-EIF3B beads is calculated relative to total mRNA isolated
846 from the cells. (**F**) Schematic of nanoluciferase reporters stably expressed in primary
847 human T cells. Nanoluciferase reporters carry the *HBB* 5'-UTR and WT, Δ*PAR,* R**PAR*
848 of the *TCRA* 3'-UTR, or Δ*PAR* of the *TCRA* 3'-UTR replaced with either a *JUN* 5'-UTR
849 hairpin or hepatitis C viral (HCV) internal ribosome entry site (domain IIIabc). (**G**)
850 Luciferase activity in anti-CD3/anti-CD28 activated T cells stably expressing
851 nanoluciferase constructs described in **F**, relative to non-activated controls. (**H**) Changes
852 in nanoluciferase mRNA levels in **G**, as determined by qRT-PCR. (**I**) Immunoprecipitation
853 as shown in **D** to quantify the amount of nanoluciferase mRNA bound to eIF3 in T cells
854 stably expressing nanoluciferase constructs in **F** after activation with anti-CD3/anti-CD28
855 antibodies for 0.5, 1, 3 and 5 hours. The percent mRNA bound to anti-EIF3B beads is
856 calculated relative to total mRNA isolated from the cells. All experiments were carried out
857 in triplicate (3 separate wells per condition), with mean and standard deviations shown.

858 All the primary human T cell experiments were performed using two donors and data from
859 one representative donor is shown.
860
861

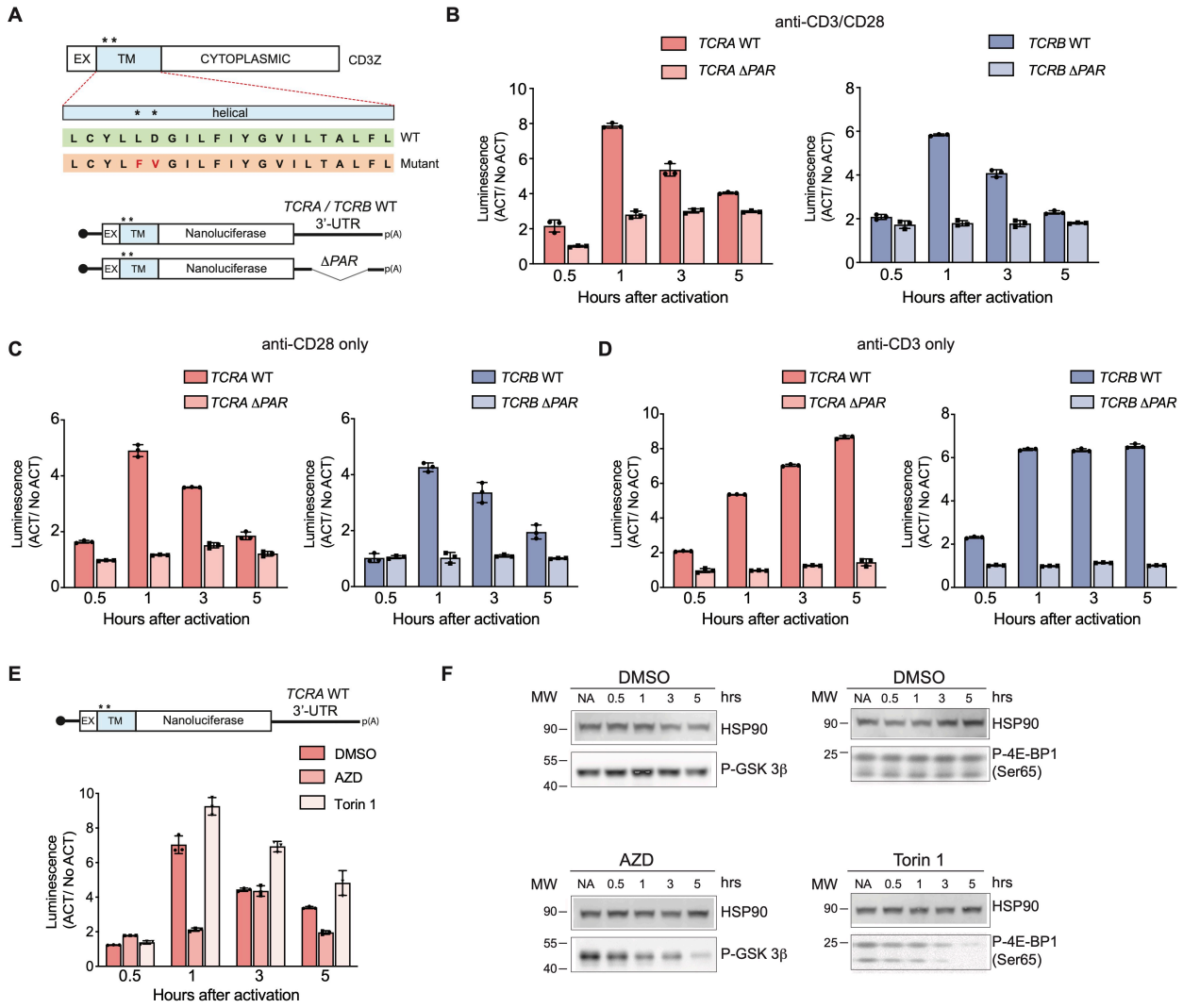

Figure 4. The burst in nanoluciferase reporter translation requires membrane-proximal CD28 signaling. (**A**) Schematic of the membrane-tethered nanoluciferase reporters stably expressed in primary human T cells. (Top) Wild-type CD3-zeta protein with asterisk indicating two amino acids mutated in the transmembrane region to prevent association with the TCR (Dong et al., 2019) (EX: extracellular, TM: transmembrane). (Bottom) Schematic of the nanoluciferase reporters. Nanoluciferase is fused C-terminal to the extracellular and transmembrane segments of CD3-zeta, mutated to prevent TCR association. The reporters carry the *HBB* 5'-UTR and *TCRA, TCRB*, *TCRA ΔPAR,* or

871 *TCRB* Δ*PAR* 3'-UTR. (**B**) Luciferase activity in primary human T cells stably expressing
872 membrane-tethered reporters described in **A** stimulated with anti-CD3/anti-CD28
873 antibodies, relative to non-activated controls (ACT/NoACT). (**C**) Luciferase activity in
874 primary human T cells stably expressing membrane-tethered reporters described in **A**,
875 and activated only with anti-CD28 antibodies, relative to non-activated controls. (**D**)
876 Luciferase activity in primary human T cells stably expressing membrane-tethered
877 reporters described in **A**, and activated only with anti-CD3 antibodies, relative to non-
878 activated controls. (**E**) Luciferase activity in primary human T cells stably expressing
879 membrane-tethered reporter with WT *TCRA* 3'-UTR described in **A** inhibited with either
880 AZD5363(AZD) to inhibit AKT activity or Torin 1 to inhibit mTOR before activating with
881 anti-CD3/anti-CD28 antibodies, relative to non-activated controls. In panels **A**–**E**, all
882 experiments were carried out in triplicate (3 separate wells per condition), with mean and
883 standard deviations shown. (**F**) Western blot carried out to measure AKT activity in the
884 presence of AZD5363 (AZD) using an anti-Phospho-GSK-3β antibody or mTOR activity
885 in the presence of Torin 1 using an anti-Phospho-4EBP1 antibody, for the samples in **E**.
886 HSP90 was used as a loading control. All the primary human T cell experiments were
887 performed using two donors and data from one representative donor is shown.

888

889

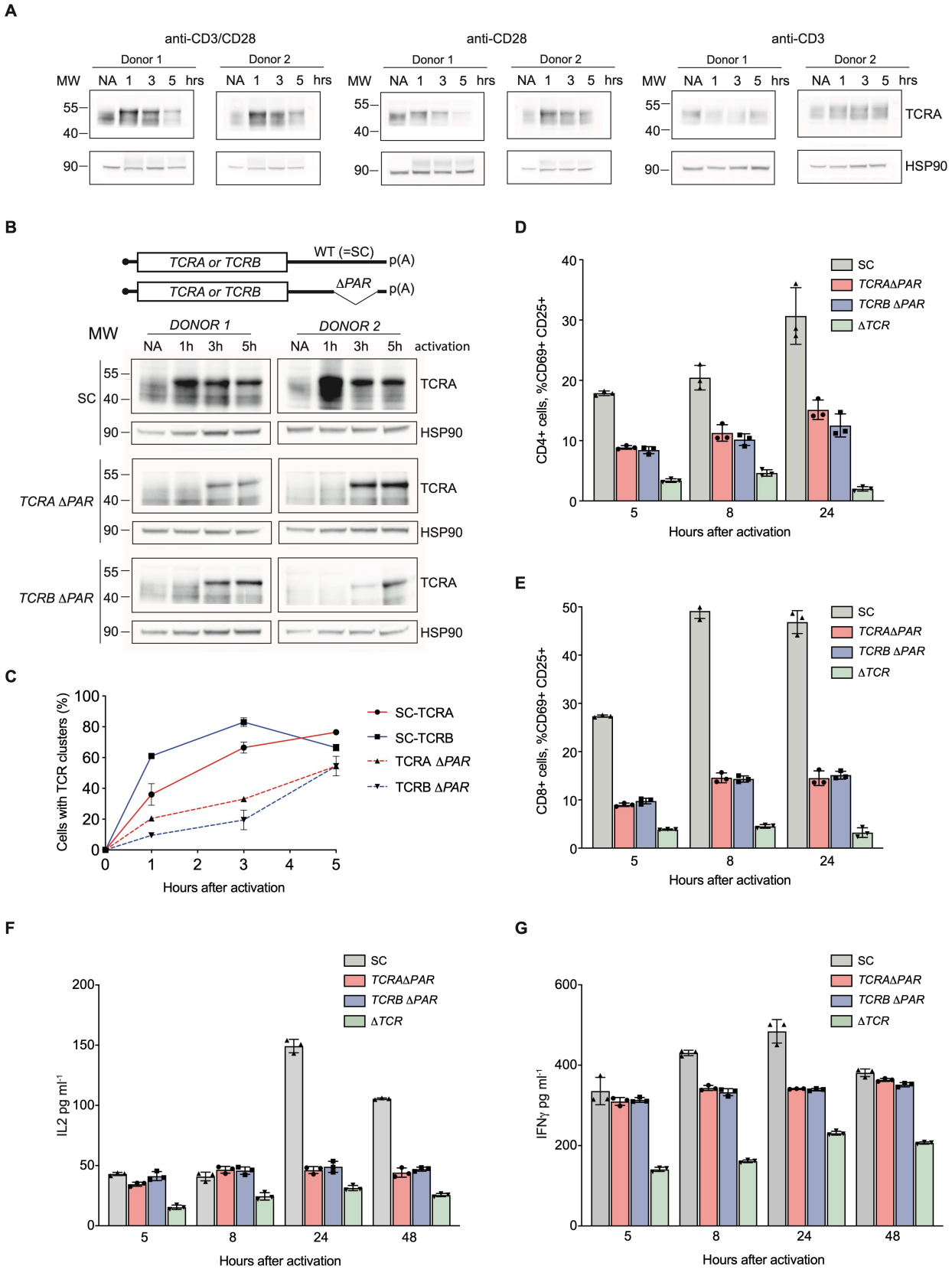
A
anti-CD3/CD28
anti-CD28
anti-CD3
Donor 1
Donor 2
MW NA 1 3 5 hrs
55
40
90
TCRA
HSP90
B
TCRA or TCRB
WT (=SC)
p(A)
ΔPAR
DONOR 1
DONOR 2
NA 1h 3h 5h activation
SC
TCRA ΔPAR
TCRB ΔPAR
C
Cells with TCR clusters (%)
Hours after activation
SC-TCRA
SC-TCRB
TCRA ΔPAR
TCRB ΔPAR
D
CD4+ cells, %CD69+ CD25+
SC
TCRAΔPAR
TCRB ΔPAR
ΔTCR
E
CD8+ cells, %CD69+ CD25+
F
IL2 pg ml-1
G
IFNγ pg ml-1

890

891 **Figure 5. eIF3 binding to the *TCRA* and *TCRB* mRNA 3'-UTR elements is required**
892 **for a rapid burst in TCR translation and robust activation of primary human T cells.**
893 (**A**) Western blots of TCRA protein levels in T cells as a function of time after different
894 modes of activation. HSP90 was used as a loading control. (**B**) Western blots measuring
895 TCRA protein levels as a function of time after anti-CD3/anti-CD28 activation. Cell lines
896 used are labeled on the left: *TCRA* Δ*PAR*, *TCRB* Δ*PAR*, and SC (scrambled gRNA).
897 HSP90 was used as a loading control. Schematics of *TCRA* and *TCRB* mRNAs with and
898 without eIF3 PAR-CLIP sites are shown above. SC control cells have the WT 3'-UTRs for
899 *TCRA* and *TCRB* mRNAs. (**C**) The number of T cells with one or more TCR clusters
900 measured by anti-TCRA/anti-TCRB protein staining and epifluorescence microscopy as
901 a function of time after anti-CD3/anti-CD28 activation. A total of 100 cells from each donor
902 were imaged for *TCRA* Δ*PAR* (*n* = 2 donors, stained with anti-TCRA antibody), *TCRB*
903 Δ*PAR* (*n* = 2 donors, stained with anti-TCRB antibody), and SC cell lines (*n* = 2 donors,
904 each stained separately with anti-TCRA and anti-TCRB antibodies). Values are mean ±
905 standard deviation. (**D**) Flow cytometric analysis measuring T cell activation markers
906 CD69 (early activation marker) and CD25 (mid-activation marker), quantifying the mean
907 percent of CD4+ T cells that are CD69+ CD25+. (**E**) Flow cytometric analysis of CD8+ T
908 cells, quantifying the mean percent of CD8+ T cells that are CD69+ CD25+. Cells sorted
909 as shown in **Figure 5–figure supplement 2**. (**F**) Quantification of IL2 secreted from SC,
910 *TCRA* Δ*PAR, TCRB* Δ*PAR* and Δ*TCR* cell populations at different time points after
911 stimulation with anti-CD3/anti-CD28 antibodies, as determined by ELISA. (**G**)
912 Quantification IFNγ secreted from the cells in **F**, as determined by ELISA. In panels **D**–**G**,

913 all experiments were carried out in triplicate (3 separate wells per condition), with mean
914 and standard deviations shown. Representative results from 1 donor are shown.
915

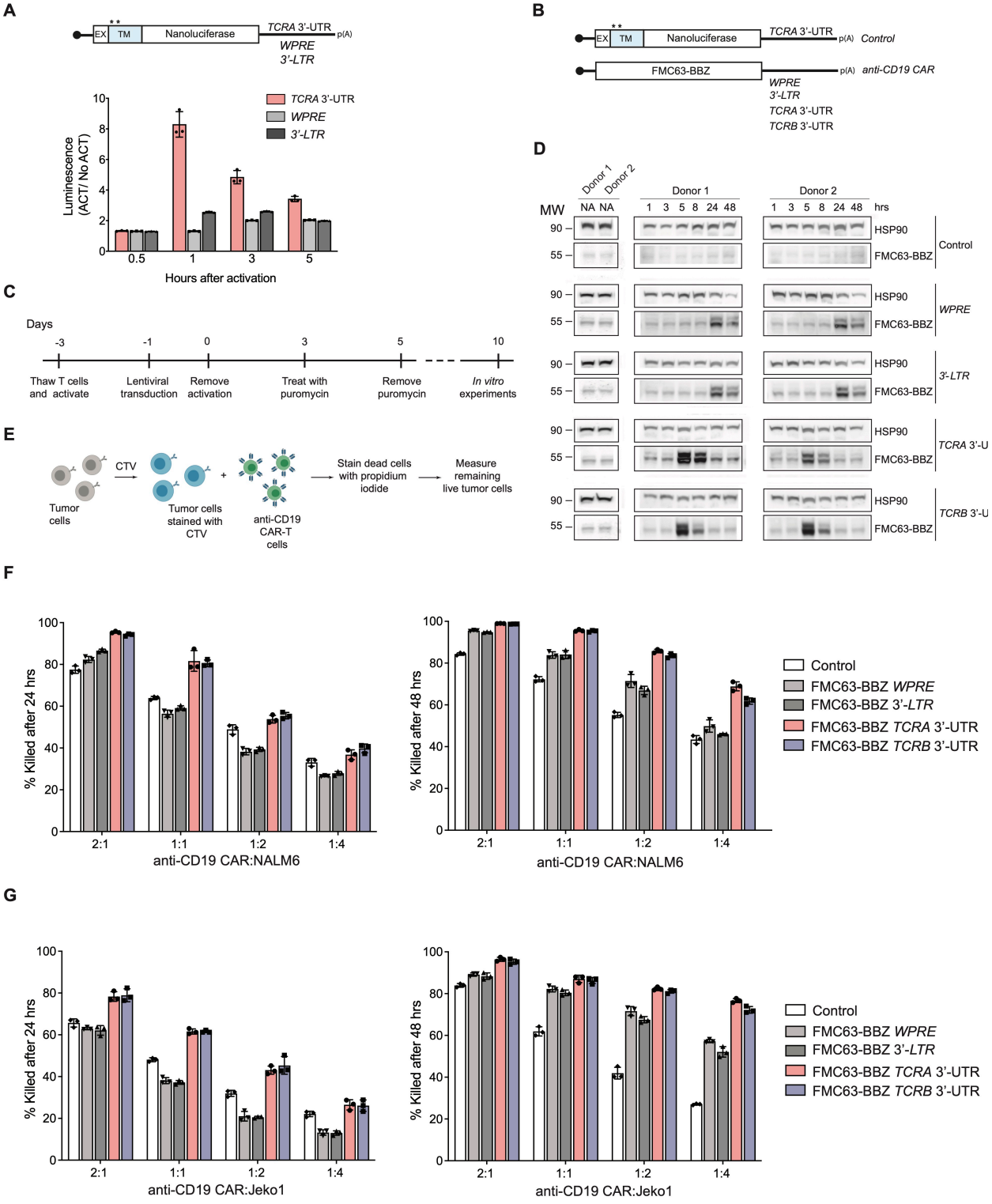

Figure 6. The *TCRA* and *TCRB* mRNA 3'-UTR elements enhance CAR T cell function. (**A**) (Top) Schematic of membrane-tethered nanoluciferase reporters stably

919 expressed in primary human T cells. The reporters have the *HBB* 5'-UTR and either the
920 *TCRA* 3'-UTR, the Woodchuck Hepatitis Virus Posttranscriptional Regulatory Element
921 (*WPRE*) or the gammaretroviral 3'-Long terminal repeat (*3'-LTR*) as 3'-UTR. (Bottom)
922 Luciferase activity in primary human T cells stably expressing membrane-tethered
923 nanoluciferase reporters described above and activated with anti-CD3/anti-CD28
924 antibodies, relative to non-activated cells. Representative results from one of two donors
925 are shown (*n* = 3 separate wells, with mean and standard deviations shown). (**B**)
926 Schematics of FMC63-BBZ CAR cDNA sequence fused 5' of the *WPRE, 3'-LTR, TCRA*
927 3'-UTR or *TCRB* 3'-UTR. The membrane-tethered nanoluciferase reporter with *TCRA* 3'-
928 UTR was used as a control for the effects of lentiviral expression. (**C**) Timeline of CAR T
929 cell generation from primary human T cells and the experiments performed. (**D**) Western
930 blots measuring FMC63-BBZ CAR protein levels as a function of time after incubation
931 with NALM6 cells. CAR T cells expressing the constructs in **B** are labeled: Control*,*
932 *WPRE, 3'-LTR, TCRA* and *TCRB* 3'-UTR. HSP90 was used as a loading control (*n* = 2
933 donors). (**E**) Schematic describing the cytotoxicity assay used to detect live tumor cells
934 after incubation with FMC63-BBZ CAR cells using flow cytometric analysis. (**F**) Cytotoxic
935 activity of FMC63-BBZ CARs fused to various 3'-UTRs described in **B** after incubating
936 with NALM6 cells for 24 and 48 hours. (**G**) Cytotoxic activity of FMC63-BBZ CARs fused
937 to various 3'-UTRs described in **B** after incubating with Jeko 1 cells for 24 and 48 hours.
938 In panels **F** and **G**, representative results for one of two donors are shown (*n* = 3 separate
939 wells, with mean and standard deviations shown).

940

941

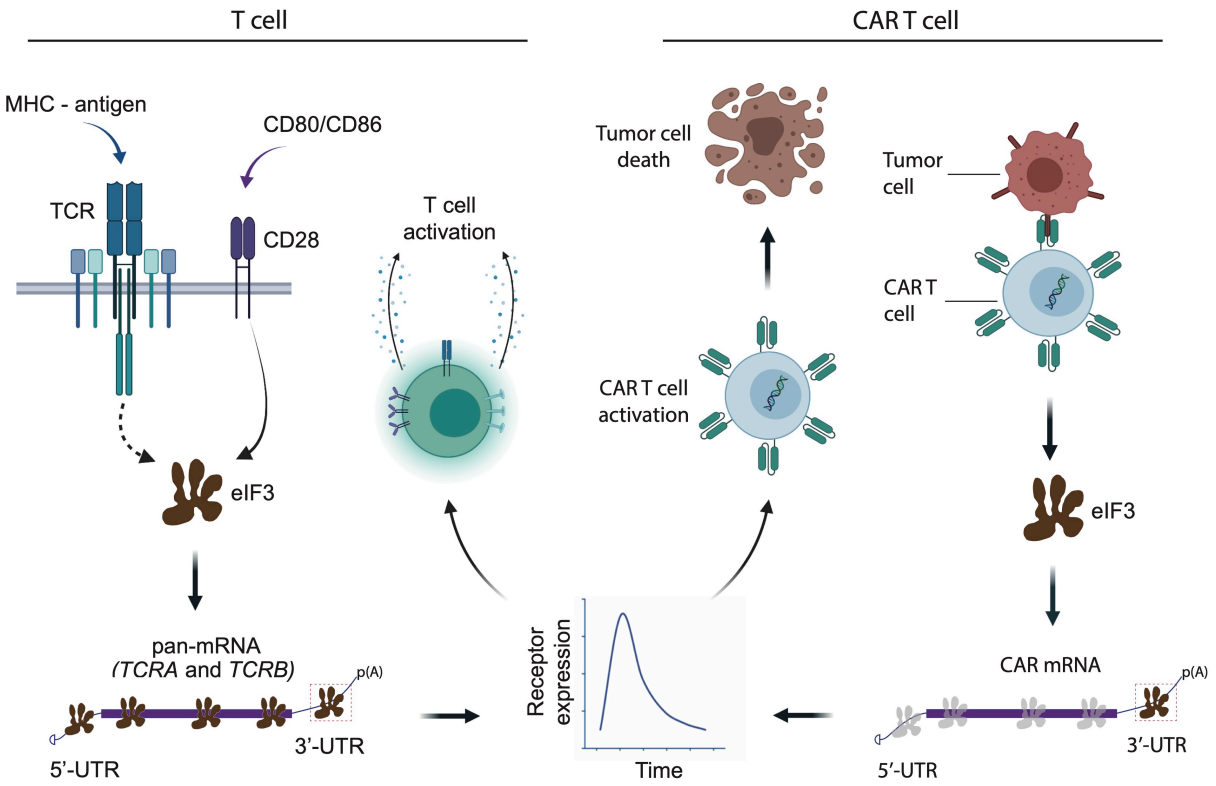

Figure 7. Model for robust T cell activation and improved CAR T cell function mediated by eIF3 interactions with the *TCRA* and *TCRB* mRNAs. Left, a T cell activated upon antigen recognition by the TCR and CD28 costimulatory signal leads to recruitment of the *TCRA* and *TCRB* mRNAs to translation "hot-spots" due to eIF3 binding to the mRNA 3'-UTRs. This results in a short burst in TCRA and TCRB translation followed by a robust increase in T cell function as measured by CD69 and CD25 expression and cytokine release. Right, activation of CAR T cells expressing CAR mRNAs with the *TCRA* or *TCRB* 3'-UTRs leads to a burst in CAR translation and improved tumor cell killing.

1

2

3 Supplementary Information for

4

5 Robust T cell activation requires a burst in T cell receptor translation 6 mediated by eIF3

7 **Authors:** Dasmanthie De Silva[1,2], Lucas Ferguson[1], Grant H. Chin[1], Benjamin E.
8 Smith[3], Ryan A. Apathy[4], Theodore L. Roth[4], Franziska Blaeschke[5], Marek Kudla[1],
9 Alexander Marson[4,5,6,7,8,9,10], Nicholas T. Ingolia[1,11], Jamie H. D. Cate[1,2,10,11,12,13]

10 Correspondence to: j-h-doudna-cate@berkeley.edu

11

12 **This PDF file includes:**

13 Materials and Methods

14 Figure supplements

15 Captions to Supplemental Files 1-6

16

17 **Other Supplemental Information for this manuscript include the following:**

18 **Supplemental Files 1-6**

19

20

21 **Materials and Methods**

22

23 Jurkat cell culture

24 Human Jurkat, Clone E6-1 (ATCC TIB-152) was purchased from American Type
25 Culture Collection (ATCC) and was maintained in RPMI 1640 Medium (ATCC
26 modification) with 10% FBS (VWR Life Science Seradigm) and 0.01% Penicillin-
27 Streptomycin (10,000 U/mL) (ThermoFisher). The cells were maintained between 1
28 million to 8 million cells/mL. When cells were stimulated they were always maintained at
29 8 million cells/mL.

30

31 Jurkat cell stimulation

32 The Jurkat cells used for the PAR-CLIP experiment were stimulated with 1X Cell
33 Stimulation Cocktail, containing phorbol 12-myristate 13-acetate (PMA) and ionomycin
34 (Thermofisher, Cat. #: 00-4970-93) to ensure a large proportion of the cells were
35 activated. Unless otherwise stated, all other experiments involving activated Jurkat cells
36 used anti-CD3/anti-CD28 antibodies (Tonbo) for stimulation. Flat bottom plates were
37 coated with anti-CD3 antibody at a 10 µg/mL concentration, and anti-CD28 antibody was
38 added to the cell culture media at a concentration of 5 µg/mL.

39

40 Isolation of human primary T cells

41 Primary human T cells were isolated from healthy human donors from
42 leukoreduction chambers after Trima Apheresis (Vitalant, formerly Blood Centers of the

43 Pacific). Peripheral blood mononuclear cells (PBMCs) were isolated from whole blood
44 samples by Ficoll centrifugation using SepMate tubes (STEMCELL) per manufacturer's
45 instructions. T cells were isolated from PBMCs from all cell sources by magnetic negative
46 selection using an EasySep Human T Cell Isolation Kit (STEMCELL), per manufacturer's
47 instructions. Unless otherwise noted, isolated T cells were stimulated with anti-CD3/anti-
48 CD28 antibodies (Tonbo) as described above and used immediately.

49

50 Primary human T cell culture

51 Bulk T cells were cultured in XVivo15 medium (Lonza) with 5% fetal bovine serum
52 (FBS), 50 μM 2-mercaptoethanol (Sigma), and 10 μM *N*-acetyl-cystine (Sigma) or
53 ImmunoCult™-XF T Cell Expansion Medium (StemCell). Immediately after isolation, T
54 cells were either frozen or stimulated for 2 days with anti-human CD3/CD28 magnetic
55 Dynabeads (ThermoFisher) at a bead to cell concentration of 1:1, along with cytokine IL-
56 2 (UCSF Pharmacy). For T cells cultured after electroporation, the media was
57 supplemented with IL-2 at 500 U/mL. Throughout the culture period T cells were
58 maintained at an approximate density of 1 million cells per mL of media. Every 2–3 days
59 after electroporation, additional media was added, along with fresh IL-2 at 500 U/mL
60 concentration, and the cells were transferred to larger culture flasks as necessary to
61 maintain a density of 1 million cells per mL. For all the other times T cells were maintained
62 at 50U/mL IL-2 with the addition of fresh media every 2 days.

63

64 Primary human T cell stimulation

65 For edited primary human T cells, the cells were transferred to fresh media lacking
66 IL-2 after 9 days of culturing. The T cells were then stimulated with anti-CD3/anti-CD28
67 antibodies using flat bottom plates coated with anti-CD3 antibody (Tonbo) at a 10 µg/mL
68 concentration, and anti-CD28 antibody (Tonbo) added to the cell culture media at a
69 concentration of 5 µg/mL. In all other primary human T cell stimulation experiments the
70 cells were stimulated with anti-CD3/anti-CD28 antibodies as mentioned above along with
71 50 U/mL IL-2.

72

73 4-thiouridine optimization for PAR-CLIP experiments

74 We used Jurkat cells as a model for T cells, as PAR-CLIP experiments require a
75 large number of cells labeled with 4-thiouridine (Sigma) at a non-toxic concentration
76 (Ascano et al., 2012). Jurkat cells also have a defined T cell receptor and transcriptome,
77 avoiding the donor-to-donor variability of primary T cells. Jurkat cells were seeded, so
78 that they reached $8X10^5$ cells ml^{-1} seeding density on the day of the experiment. Varying
79 concentrations of 4-thiouridine (s4U) were added to the cells (50 µM, 75 µM, 100 µM, or
80 none as a negative control). The cells were then incubated for different time points: 8
81 hours, 10 hours, 12 hours, or 16 hours. After each incubation time cell viability was
82 determined using the CellTiter-Glo assay (Promega), according to the manufacturer's
83 instructions. Concentrations at which the relative luminescence in the presence of s^4U
84 (luminescence of the s^4U treated cells/luminescence of the untreated cells) exceeded
85 95% were considered non-toxic. Based on these measurements, we used 50 µM of 4-
86 thiouridine for PAR-CLIP experiments.

87

88 PAR-CLIP

89 Two biological replicates were used to perform PAR-CLIP analysis as described
90 in (Lee et al., 2015), with modifications for Jurkat cells. 50 μM of 4-thiouridine was
91 determined as non-toxic to Jurkat cells over the time course of the PAR-CLIP experiments
92 (Ascano et al., 2012). A total of 55 million Jurkat cells seeded at 8 million cells ml^{-1} was
93 treated with 50 μM of 4-thiouridine for 7 hours, then stimulated with 1X Cell Stimulation
94 Cocktail for 5 hours in media containing 50 μM of 4-thiouridine (**Figure 1A**). The same
95 number of cells were treated with 50 μM of 4-thiouridine for 12 hours without stimulation
96 as a non-activated control. The cells were then crosslinked on ice with 365 nm UV
97 irradiation at an energy dose of 0.2 J cm^{-2}. The cells were pelleted by centrifugation at
98 100 x g for 15 min at 4 °C, and the pellet was resuspended in three volumes of NP40 lysis
99 buffer (50 mM HEPES-KOH pH 7.5, 150 mM KCl, 2 mM EDTA, 0.5% Nonidet P-40
100 alternative, 0.5 mM dithiothreitol (DTT), 1 Complete Mini EDTA-free Protease Inhibitor
101 Cocktail tablet (Roche)). The cell suspension was then incubated on ice for 10 min,
102 passed through an 18G needle five times, and centrifuged at 13,000 x g for 15 min at 4
103 °C and RNAs were lightly digested by treatment with MNase (Thermo Scientific) at a final
104 concentration of 0.05 U μl^{-1} for 20 min at 16 °C. For each PAR-CLIP assay 1000 μl of
105 Dynabeads (Invitrogen) and 800 μl of anti-EIF3B antibody (Bethyl A301-761A) were used.
106 The remaining steps of the PAR-CLIP analysis were performed exactly as described in
107 (Danan et al., 2016; Lee et al., 2015) with the exception of using MNase at 5 U μl^{-1} for the
108 on-bead digestion step.

109

110 Mass spectrometry

111 To identify eIF3 subunits that crosslinked with RNAs in the PAR-CLIP experiments,
112 a portion of eIF3 immunoprecipitated using Dynabeads as described above were treated
113 with nonradioactive ATP (NEB) during the T4 polynucleotide kinase labeling step. The
114 nonradioactive samples were then run on the same gel next to the radiolabeled PAR-
115 CLIP samples, Coomassie stained (Pierce) and the bands that matched with the
116 phosphorimager printout were excised from the gel and submitted for identification using
117 one-dimensional LC-MS/MS (**Supplementary File 1**).

118

119 PAR-CLIP computational analysis

120 PAR-CLIP cDNA libraries were sequenced on an Illumina HiSeq 2500 platform.
121 To eliminate potential PCR biases during PAR-CLIP library preparation, a random bar
122 code was introduced into the 3' adapter and all the reads that matched the random
123 barcode were collapsed into single reads. Clusters of overlapping sequence reads
124 mapped against the human genome version hg38 were generated using the PARalyzer
125 software (Corcoran et al., 2011) incorporated into the PARpipe pipeline
126 (https://ohlerlab.mdc-berlin.de/software/PARpipe_119/, (Mukherjee et al., 2019) with the
127 settings below. Binding sites were categorized using the Gencode GRCh38.p12 GTF
128 annotations (gencode.v21.annotation.gtf), https://www.gencodegenes.org/human/.

129

130 The PARpipe settings used were:

131 Conversion = T>C

132 Minimum read count per group = 5

133 Minimum read count per cluster = 7

134 Minimum read count for kde = 3

135 Minimum cluster size = 11

136 Minimum conversion locations for cluster = 2

137 Minimum conversion count for cluster = 2

138 Minimum read count for cluster inclusion = 1

139 Minimum read length = 20

140 Maximum number of non conversion mismatches = 1

141

142 Comparison of eIF3 PAR-CLIP results in Jurkat and HEK293T cells

143 To compare RNAs in activated Jurkat cells crosslinked to eIF3 with those
144 crosslinked to eIF3 in HEK293T cells (Lee et al., 2015), the gene cluster lists
145 (*.gene_cl.csv) from APA_REP1, APA_REP2, APB_REP1, APB_REP2, APD_REP1,
146 and APD_REP2 were used (see **Supplementary File 3**). The genes were first sorted by
147 total read counts ("ReadCountSum") from high to low for each library to obtain the top
148 candidate genes. Then, the same number of top candidate genes from these sorted lists
149 as the number of genes identified in HEK293T cells, for eIF3 subunit EIF3A, EIF3B, and
150 EIF3D crosslinked to RNA (Lee et al., 2015), were chosen for comparison.

151

152 PAR-CLIP Pathway analysis

153 To determine biological pathways enriched in the set of mRNAs that crosslinked
154 to eIF3 in activated Jurkat cells, genes with at least 100 total aligned reads were used,
155 as determined in the PARpipe analysis described above (Mukherjee et al., 2019), from
156 the EIF3A/C/B samples. Since PAR-CLIP reads are short, it is not possible to determine
157 with certainty which mRNA transcript isoform cross-linked with eIF3. Therefore the most
158 abundant mRNA transcript isoform for each gene was chosen, as determined by
159 transcriptome profiling using kallisto (protein_coding category) (Bray et al., 2016), as
160 described in the Transcriptome Profiling section. Even with this choice, eIF3 crosslinks to
161 mRNAs do not correlate with mRNA abundance (**Figure 1–figure supplement 1F**).
162 Human genome GRCh38.p13 annotation was used to extract mRNA lengths by 5'-UTR,
163 coding region and 3'-UTR (Ensembl Biomart) (Cunningham et al., 2019). These genes
164 were then sorted by the density of PAR-CLIP reads in the mRNA 5'-UTR region, prior to
165 mapping pathways of transcripts that crosslinked to eIF3. Due to the complexity of *TCRA*
166 and *TCRB* transcript annotation, these transcripts were excluded from the normalization
167 calculation, but included in the pathway analysis. The top 500 genes from the resulting
168 EIF3A/C/B PAR-CLIP gene lists were used, sorted as described above, to analyze gene
169 enrichment profiles in the STRING database (Szklarczyk et al., 2019). The top tissue-
170 specific categories involve the immune system and T cell function (**Supplementary File**
171 **5**). Note that the STRING database categories are not mutually exclusive gene lists, and
172 do not include TCR subunits in its analysis.

173

174 <u>Metagene analysis</u>

175 The PAR-CLIP genes sorted as described above in the "PAR-CLIP pathway
176 analysis" were used and mapped against the most abundant mRNA transcript isoforms
177 to generate cumulative plots of the reads. Reads for the *TCRA* and *TCRB* mRNAs were
178 manually extracted from the Bowtie version 1.0.0 Hg38 alignment of the eIF3 PAR-CLIP
179 reads. We did not identify reads mapped to the D segment of *TCRB* (e.g. to *TRBD2*) due
180 to its short length of 16 nucleotides. These reads were combined with the mapped reads
181 in the *.read.csv files generated by Parpipe. The combined reads were then sorted to
182 extract only reads annotated as 5'-UTR, start codon, coding, stop codon, and 3'-UTR.
183 The most abundant transcript isoform, as identified in the Transcriptome Profiling section
184 using kallisto (described below) was used. Reads mapped to the 5'-UTR and start codon
185 were normalized by the length of the 5'-UTR. Reads mapped to the coding region and
186 stop codon were normalized by the length of the coding region. Finally, reads mapped to
187 the 3'-UTR were normalized to the length of the 3'-UTR. Relative positions of the mapped
188 reads along a metagene were computed based on the locations each mapped read fell
189 within its respective feature. Relative positions were from -1 to 0 for the 5'-UTR, 0 to 1 for
190 the coding region, and 1 to 2 for the 3'-UTR. 5'-UTR values were computed by multiplying
191 the relative position by -1, whereas the 3'-UTR values were computed by adding 1 to the
192 relative position. Coding region relative positions were unchanged.

193 The empirical cumulative distribution frequency function from R package ggplot2
194 (Wickham et al., 2016) was used to build the metagene plots from the vector of relative
195 positions for the reads which mapped to a given set of reads. We defined mRNAs having
196 a ratio of normalized 5'-UTR reads divided by 3'-UTR reads of 20 or more as "5'-UTR
197 enriched" with respect to eIF3 crosslinking. All others were categorized as "pan-mRNAs,"

198 with eIF3 crosslinking across the entire length of the mRNA. The cut-off value 20 is not a
199 sharp boundary between the two categories of mRNA (**Figure 1–figure supplement 1G**).
200

201 Transcriptome Profiling

202 RNA samples were extracted from non-activated Jurkat cells or Jurkat cells activated for
203 5 hr with I+PMA, using the Direct-zol RNA Miniprep kit (Zymoresearch). The libraries were
204 prepared using TruSeq Stranded RNA LT Ribo-Zero Gold kit (Illumina) following the
205 manufacturer's instructions, with two biological replicates. Cutadapt (version 2.6) (Martin,
206 2011) with a minimum read length of 20, 5' end with a cutoff of 15 and the 3' end with a
207 cutoff of 10 in paired-end mode was used to remove adapters. RNA-seq reads were
208 pseudoaligned using kallisto v.0.46.0 run in quant mode with default parameters to
209 estimate transcript abundance (transcripts per million, TPM) (Bray et al., 2016). The
210 transcript index for kallisto was made with default parameters and GENCODE Release
211 32 (GRCh38.p13) FASTA file (Frankish et al., 2019).
212

213 RNA-FISH and immunofluorescence

214 Jurkat cells were washed with PBS, fixed with 3.7% (vol./vol.) paraformaldehyde
215 (VWR) for 10 min at room temperature and washed three times with PBS. PBS was
216 discarded and 1 ml 70% ethanol was added. The cells were incubated at 4°C for 16 hours.
217 The 70% ethanol was aspirated and the cells were washed once with 0.5 ml Stellaris RNA
218 wash buffer A (Biosearch technologies). The cells were then incubated with 100 µl
219 Stellaris hybridization buffer (Biosearch Technologies) containing Stellaris RNA FISH

220 probes (Biosearch Technologies) at a final concentration of 125 nM (**Supplementary File**
221 **6)** and with the relevant antibody (**Supplementary File 6**) for 16 hours at 28 °C. The cells
222 were then washed twice with 0.5 ml Stellaris RNA wash buffer A containing secondary
223 antibody conjugated with a fluorophore for 30 minutes at 37 °C in the dark. The second
224 Stellaris RNA wash buffer A contained DAPI in addition to the secondary antibody. Finally
225 the cells were washed once with 0.5 mL Stellaris RNA wash buffer B and mounted with
226 mounting solution (Invitrogen). All high resolution images were taken using confocal
227 ZEISS LSM 880 in Airyscan super-resolution mode, equipped withA Plan-Apochromat
228 63x/1.4 Oil objective (Zeiss). To measure colocalization of *TCRA* and *TCRB* mRNAs with
229 each other or with P bodies (using DCP1 antibody, **Supplementary File 6**) or stress
230 granules (G3BP1 antibody, **Supplementary File 6**) the cells were mounted along with
231 0.1 µm TetraSpeck™ microspheres (ThermoFisher) adhered to the slide according to
232 manufacturer's instructions, to be able to account for the chromatic shift during image
233 acquisition.

234

235 <u>Colocalization analysis</u>

236 To measure colocalization of *TCRA* and *TCRB* mRNAs with each other or with P
237 bodies (using DCP1 antibody) or stress granules (G3BP1 antibody), immunofluorescently
238 labelled cells (see above) were mounted along with 0.1 µm TetraSpeck™ microspheres
239 (ThermoFisher) adhered to the slide according to manufacturer's instructions. The
240 microspheres allowed for the correction of lateral and axial chromatic aberrations during
241 image acquisition.

242 Z-stacks were acquired with 35 nm x 35 nm x 190 nm voxels on a ZEISS LSM 880
243 in Airyscan super-resolution mode, equipped with a Plan-Apochromat 63x/1.4 Oil
244 objective (Zeiss). The images were then deconvolved to a lateral resolution of ≈150 nm
245 and an axial resolution of ≈500 nm (as confirmed by observing the discrete Fourier
246 transform of the z-stacks). After imaging a single cell, beads that were on the slide axial
247 to the cell were imaged to measure the corresponding lateral and axial chromatic
248 aberrations.

249 To quantify the relative colocalization, we developed an automated processing and
250 analysis pipeline in ImageJ 1.52p available on github:
251 https://github.com/Llamero/TCR_colocalization_analysis-macro. Specifically, the
252 chromatic aberrations in the z-stacks were compensated for by registering the channels
253 of the bead z-stack to one another, and then applying the same registration vectors to the
254 corresponding channels in the cell z-stack (Parslow et al., 2014). Each channel of a z-
255 stack was then thresholded to remove background in the image, and then the
256 colocalization between each pair of images was measured using the Pearson's
257 correlation coefficient. Samples in which any pair of channels in the bead z-stack had a
258 correlation of less than 0.45 were removed from final analysis, as this suggested that the
259 images had insufficient dynamic range in at least one of the channels for an accurate
260 deconvolution.

261

262 Polysome analysis of eIF3-associated mRNAs

263 To isolate polysomes from Jurkat cells, the cells were seeded to reach 8 x 10^5
264 cells/mL on the day of harvest and then stimulated with anti-CD3/anti-CD28 antibodies as

265 described above for 5 hours. To isolate polysomes from primary human T cells, the cells
266 were seeded to reach 1 x 10^6 cells/mL on the day of harvest and then stimulated with anti-
267 CD3 and anti-CD28 antibodies as described above for 1 hour. Both Jurkat and primary
268 human T cells were treated with 100 µg ml^{-1} cycloheximide (VWR) 5 minutes before
269 harvesting. Cells were then collected into a 50 ml falcon tube and rinsed once with ice
270 cold PBS (ThermoFisher) supplemented with 100 µg ml^{-1} cycloheximide. The cells were
271 then incubated with 0.5 mM of the crosslinking reagent dithiobis (succinimidyl propionate)
272 (DSP, Thermofisher, Cat. #: PG82081) and 100 µg ml^{-1} cycloheximide in PBS at room
273 temperature for 15 minutes, with rocking. The crosslinking reagent was then removed and
274 the cells were incubated with quenching reagent (PBS, 100 µg ml^{-1} cycloheximide and
275 300 mM Glycine(Sigma)) for 5 minutes on ice. The cells were then rinsed again with ice
276 cold PBS and flash frozen in liquid nitrogen.

277 A total of 4 x 10^8 cells were lysed with 400 µl hypotonic lysis buffer (10 mM Hepes
278 pH 7.9, 1.5 mM $MgCl_2$, 10 mM KCl, 0.5 mM DTT, 1% Triton, 100 µg ml^{-1} cycloheximide,
279 and one Complete EDTA-free Proteinase Inhibitor Cocktail tablet (Roche)). The cells
280 were incubated for 10 min on ice and then passed through an 18G needle five times, and
281 centrifuged at 13,000 × g for 15 min at 4 °C. The 400 µl supernatant was then transferred
282 to a fresh eppendorf tube and subjected to RNase H digestion by adding the following
283 reagents: 3 mM $MgCl_2$, 10 mM DTT, 200 units RNase H (NEB) and 20 µl of SUPERasIN
284 (ThermoFisher), with a total of 4 µM DNA oligos (IDT), as indicated in the figure legends.
285 The mixture was then incubated at 37 °C for 20 minutes. After incubation 10 µl of the
286 RNase H treated lysate mixture was isolated to test the efficiency of the RNase H
287 digestion using qRT-PCR (**Figure 2–figure supplement 1B, 1D, and 1G**) and the rest of

288 the lysate was layered onto a 12 ml 10%-50% sucrose gradient, made with gradient buffer
289 consisting of: 10% sucrose (w/v) or 50% sucrose (w/v), 100 mM KCl, 20 mM Hepes pH
290 7.6, 5 mM $MgCl_2$, 1 mM DTT and 100 µg ml^{-1} cycloheximide. The gradient was centrifuged
291 at 36,000 rpm (222k x g) for 2 hours at 4 °C in a SW-41 rotor. The gradient was then
292 fractionated using the Brandel gradient fractionator and ISCO UA-6 UV detector and all
293 the polysome fractions (~ 5 ml) were collected into a fresh 15 ml falcon tube. 100 µl from
294 each of the polysome fractions was kept aside to measure the input RNA amounts, and
295 the rest of each polysome fraction was incubated with 100 µl of Dynabeads (Invitrogen)
296 conjugated with 40 µl of anti-EIF3B antibody (Bethyl A301-761A) for 16 hours, rotating at
297 4 °C. After incubation, the beads were rinsed three times with 1000 µl room temperature
298 NP40 lysis buffer (defined in the PAR-CLIP section), rotating for 5 minutes for each wash.
299 After the final wash the beads were resuspended in 400 µl of Trizol (Thermofisher), the
300 RNA was extracted and qRT-PCR was performed as described above.

301

302 Western Blot

303 Western blot analysis was performed using the antibodies listed in
304 **Supplementary File 6**.

305

306 Total mRNA isolation and quantitative RT-PCR analysis

307 Total RNA was isolated from whole cells for qRT-PCR using Quick RNA miniprep
308 plus kit from Zymo Research following the manufacturer's instructions. Quantitative RT-
309 PCR analysis was performed using the Power SYBR Green RNA-to-Ct 1-Step kit (Applied

310 Biosystems) according to the manufacturer's instructions, and the QuantStudio™ 3 Real-
311 Time PCR System (ThermoFisher). Each target mRNA was quantified in three biological
312 replicates, with each biological replicate having three technical replicates.

313

314 Plasmids

315 Nanoluciferase reporters (Hall et al., 2012) were constructed using the 5'-UTR of
316 the human beta globin mRNA (*HBB*) and a PEST destabilization domain. The PEST
317 domain reduces protein half-life (Voon et al., 2005) and was used to provide better time
318 resolution of nanoluciferase expression after T cell activation. The *TCRA* 3'-UTR and
319 *TCRB* 3'-UTR sequences were amplified from Jurkat genomic DNA. The nanoluciferease
320 sequence fused to a PEST domain was amplified from pNL1.2[*NlucP*] Vector Sequence
321 (Promega) and was cloned into a modified CD813A vector (System Biosciences) using
322 the In-Fusion® HD Cloning Kit (Takara). The subsequent mutations in the *TCRA* and
323 *TCRB* 3'-UTRs were generated using these initial constructs. For *TCRA* Δ*PAR*
324 constructs, nucleotides 102-338 in the 3'-UTR of *TCRA* mRNA were deleted. For *TCRB*
325 Δ*PAR* constructs, nucleotides 16-161 in the 3'-UTR of *TCRB* mRNA were deleted.
326 *TCRA/TCRB* Δ*PAR*, *TCRA/TCRB R*PAR, 3'-LTR* (3'-Long Terminal Repeat), *JUN* 5'-
327 UTR hairpin (**Supplementary File 6**) and HCV IRES domain III (**Supplementary File 6**)
328 sequences were purchased as gblocks from IDT and were cloned into this plasmid
329 backbone. The *WPRE* (Woodchuck Hepatitis Virus Posttranscriptional Regulatory
330 Element) 3'-UTR sequence was amplified from the CD813A-1 (System Biosciences)
331 vector.

332 For nanoluciferase reporters designed to be membrane-tethered, we fused the N-
333 terminal sequence of CD3-zeta spanning the transmembrane helix (amino acids 1-60)
334 ordered as a gblocks from IDT to the nanoluciferase sequence above. To prevent
335 interaction of the CD3-zeta-nanoluciferase fusion protein with the TCR, we made
336 mutations in the CD3-zeta derived transmembrane helix that would disrupt interactions
337 with the TCR, based on the cryo-EM structure of the complex (Dong et al., 2019) (PDB
338 entry 6JXR) and consistent with earlier biochemical results (Call et al., 2002). The two
339 mutations, L35F and D36V, are predicted to introduce a steric clash and disrupt an intra-
340 membrane salt bridge, respectively, with other subunits in the TCR holo-complex. These
341 CD3-zeta-nanoluciferase chimeras were cloned into the modified CD813A plasmids
342 described above.

343

344 <u>Generation of primary human T cells stably expressing nanoluciferase reporters</u>

345 For lentiviral production, HEK293T cells were plated at a density of 80% in T-75
346 flasks the night before transfection. The cells were then transfected with plasmids:
347 expressing the nanoluciferase, PsPAX2 and pCMV-VSV-G using the Lipofectamine 2000
348 reagent (ThermoFisher) following the manufacturer's instructions. Forty-eight hours after
349 transfection, the viral supernatant was collected, filtered and concentrated using PEG-it
350 Virus Precipitation Solution (System Biosciences) following the manufacturer's
351 instructions. The virus pellets were then resuspended in ImmunoCult™-XF T Cell
352 Expansion media and stored in -80 °C.

353 The primary human T cell transductions were done with multiple viral titers using
354 TransDux™ MAX Lentivirus Transduction Reagent (System Biosciences) following the
355 manufacturer's instructions. To test the viral transduction efficiency of the cells, forty-eight
356 hours after viral transduction the percent of cells expressing GFP was measured by FACS
357 analysis and cells expressing less than 30% GFP were treated with 1 μg ml^{-1} puromycin
358 (ThermoFisher) for 4 days or until ~90% of the cells are GFP positive.

359

360 Luciferase reporter assays

361 The stable cell lines expressing the Nanoluciferase reporters were stimulated with
362 anti-CD3/anti-CD28 antibodies with 50 U/mL IL-2 and the nanoluciferase activity was
363 assayed after 30 min, 1 hr, 3 hr, and 5 hr after stimulation using Nano-Glo® Luciferase
364 Assay System (Promega). For each time point 200,000 cells were tested in triplicate for
365 each cell line.

366 For assays of TCR and CD28 signaling requirements, the stable cell lines were
367 stimulated with anti-CD3 or anti-CD28 antibodies individually in the presence of 50 U/mL
368 IL-2, and assayed as described above. To identify signaling pathways downstream of
369 CD28, cells were incubated with AKT inhibitor AZD5363 at 1 μM (Cayman Chemical),
370 mTOR inhibitor Torin1 250 nM (Cayman Chemical) or DMSO for 3 hours prior to T cell
371 activation with anti-CD3/anti-CD28 antibodies (Tonbo) as indicated above. The cells were
372 assayed as described above, and the extent of AKT and mTOR inhibition were
373 determined by western blot analysis of phosphorylation of their substrates GSK-3β and
374 4E-BP1, respectively.

375

376 RNA immunoprecipitation and qPCR

377 The EIF3B-RNA immunoprecipitations were carried out following the exact same
378 conditions used for the PAR-CLIP analysis with the following changes. For each
379 immunoprecipitation, cell lysates were prepared in NP40 lysis buffer (defined in the PAR-
380 CLIP section) with 4 million cells. The lysates were then incubated with 50 µl Protein G
381 Dynabeads conjugated with 20 µl of anti-EIF3B antibody (Bethyl A301-761A) for two
382 hours at 4 °C. After incubation, the flow through was removed and the beads were washed
383 three times with 1 ml NP40 lysis buffer for each wash. The beads were then resuspended
384 in 400 µl TRIzol reagent (ThermoFisher) and vortexed for 1 minute. The RNA was
385 extracted following the manufacturer's instructions and qPCR was performed as
386 described above using primers listed in **Supplementary File 6**.

387

388 sgRNA/Cas9 RNP production

389 The sgRNA/Cas9 RNPs used to edit Jurkat cells were produced by complexing
390 sgRNA (Synthego) to Cas9 as described (Schumann et al., 2015) while RNPs to edit
391 Primary Human T cells were produced by complexing a two-component gRNA (crRNA
392 and tracrRNA, Dharmacon) to Cas9 as described in (Roth et al., 2018). The targeting
393 sequences for the sgRNAs and crRNA are given in **Supplementary File 6**. Recombinant
394 Cas9-NLS was obtained from MacroLab in the California Institute for Quantitative
395 Biosciences.

396

397 Primary T cell and Jurkat genome editing

398 Jurkat cells used for electroporation were collected at passage 5 or lower and were
399 maintained at a seeding density of 8 million cells/mL or lower. Primary T cells were
400 isolated as described above. Prior to electroporation the Primary T cells were stimulated
401 with magnetic anti-CD3/anti-CD28 Dynabeads (ThermoFisher) for 48 hours. After 48
402 hours these beads were removed from the cells by placing cells on an EasySep cell
403 separation magnet for 2 min before electroporation. One million Jurkat (not activated) or
404 primary T cells cells (activated with anti-CD3/anti-CD28 Dynabeads for 48 hours) were
405 rinsed with PBS and then resuspended in 20 µl of Lonza electroporation buffer P3. The
406 cells were then mixed with 2.5 µl Cas9 RNPs (50 pmol total) along with 2 µl of a 127-
407 nucleotide non-specific single-stranded DNA oligonucleotide at 2 µg μl^{-1} (4 µg ssDNA
408 oligonucleotide total). The cells were then electroporated per well using a Lonza 4D 96-
409 well electroporation system with pulse code DN100 for Jurkat cells and EH115 for primary
410 human T cells. Immediately after electroporation, 80 µl of pre-warmed media (without
411 cytokines) was added to each well, and the cells were allowed to rest for 15 min at 37 °C
412 in a cell culture incubator while remaining in electroporation cuvettes. After 15 min, cells
413 were moved to final culture flasks. Jurkat cells were clonally selected by single cell sorting
414 into U-bottomed 96 well plates and by testing each clone using PCR primers flanking the
415 editing site (**Figure 5–figure supplement 1A**). The clones producing a single PCR band
416 of 1283 bp and 1022 bp were selected as clonal populations for *TCRA* Δ*PAR* and *TCRB*
417 Δ*PAR* respectively.

418 Genome edited populations of primary T cells with the *TCRA* Δ*PAR* and *TCRB*
419 Δ*PAR* mutations were determined by measuring the density of the PCR bands described

420 above resulting from the edited cell population compared to the PCR band from non
421 edited cells, using ImageJ. To compare with the *TCRA* Δ*PAR* or *TCRB* Δ*PAR* primary T
422 cell populations, we edited cells from both donors using each gRNA targeting the *TCRA*
423 3'-UTR and *TCRB* 3'-UTR region separately (single gRNA experiments), a gRNA
424 targeting the coding sequence (CDS) of *TCRA* which knocks out TCR expression with
425 high efficiency (Δ*TCR*) (Roth et al., 2018), a scrambled gRNA (SC) which does not target
426 any site in the human genome, and cells mixed with the gRNA/Cas9 RNPs but not
427 nucleofected.

428

429 Analysis of TCR cluster formation

430 WT, *TCRA ΔPAR* or *TCRB ΔPAR* T cells were activated with anti-CD3/anti-CD28
431 antibodies for 1, 3 or 5 hours, as described above. Cells were collected and stained with
432 anti-TCRA antibodies, followed by a secondary antibody Alexa Fluor 488 goat anti-mouse
433 IgG (Invitrogen). For the counting of cells containing TCR clusters, immunofluorescent
434 imaging was performed on a Revolve Epi-Fluorescence microscope (Echo), equipped
435 with an A Plan-Apochromat 40x objective (Olympus). Cells with substantial puncta
436 (arrows in **Figure 5–figure supplement 1C**) were scored as having TCR cluster
437 formation (**Figure 5C**).

438

439 Flow cytometry and cell sorting

440 Flow cytometric analysis was performed on an Attune NxT Acoustic Focusing
441 Cytometer (ThermoFisher). Surface staining for flow cytometry and cell sorting was

442 performed by pelleting cells and resuspending in 50 µl of FACS buffer (2% FBS in PBS)
443 with antibodies at a 1:100 concentration (**Supplementary File 4**) for 20 min at 4 °C in
444 the dark. Cells were washed twice in FACS buffer before resuspension and analysis.

445

446 ELISA

447 The cell culture supernatants were collected after each time point of activation with
448 anti-CD3/anti-CD28 antibodies for WT, *TCRA ΔPAR* or *TCRB ΔPAR* cells. For each
449 timepoint the same number of cells were used from each strain to be able to compare
450 across strains and time points. The amount of secreted IL-2 in the cell suspensions after
451 activation anti-CD3/anti-CD28 antibodies for WT, *TCRA ΔPAR* or *TCRB ΔPAR* cells were
452 measured by ELISA MAX™ Deluxe Set Human IL-2 (BioLegend) according to the
453 manufacturer's instructions.

454

455 Chimeric antigen receptor (CAR) construct sequences

456

457 The CDS region of the Juno anti-CD19 chimeric antigen receptor presently used
458 in the clinic (June et al., 2014; Kalos et al., 2011) was cloned into CD813A lentiviral
459 vectors (Systems Biosciences) with a common core EF1alpha promoter and 5'-UTR
460 with an inserted intron. The CDS sequence was followed by various 3'-UTRs. Two of
461 the 3'-UTRs are presently used in clinical CAR T cells, the Woodchuck Hepatitis Virus
462 Posttranscriptional Regulatory Element (*WPRE*) (June et al., 2014; Milone et al., 2009),
463 or the murine stem cell virus (MSCV) retroviral 3'-long terminal repeat (*3'-LTR*)

464 (Kochenderfer et al., 2009). We also cloned the full *TCRA* or *TCRB* 3'-UTR sequences
465 including the polyadenylation sites after the anti-CD19 CAR CDS sequence.
466
467 Production of CAR T cells
468
469 Production of the CAR-expressing lentiviruses was carried out as described
470 above using HEK293T cells. The viruses were then concentrated using PEG-it Virus
471 Precipitation Solution (System Biosciences) following the manufacturer's instructions.
472 The virus pellets were then resuspended in ImmunoCult™-XF T Cell Expansion media
473 and stored in -80 °C. Frozen primary human T cell pellets were thawed and then
474 stimulated with ImmunoCult™ Human CD3/CD28/CD2 T Cell Activator (Stemcell) for 48
475 hours and then transduced with various CAR viruses using TransDux™ MAX Lentivirus
476 Transduction Reagent (System Biosciences) as described above. Two days after
477 transduction the percent of cells expressing GFP was measured by FACS analysis and
478 cells expressing less than 30% GFP were treated with 1 µg mL^{-1} puromycin
479 (ThermoFisher) for 2 days or until ~90% of the cells are GFP positive. After removal of
480 puromycin the cells were seeded at $1x10^6$ cells/mL upto 9 days from the day the cells
481 were transduced by adding fresh ImmunoCult™-XF T Cell Expansion Medium
482 (StemCell) and 50 U/mL IL-2 every other day. After 9 days the CAR T cells were used
483 for various assays.
484
485 CAR expression dynamics

486 To measure CAR expression dynamics by western blot analysis, CAR T cells
487 were incubated with NALM6 tumor cells at a ratio of 1:2 CAR T cell:NALM6 cells, in
488 ImmunoCult™-XF T Cell Expansion Medium (StemCell) and 50 U/mL IL-2. Cells were
489 collected at the indicated time points and processed for western blot analysis as
490 described above. The total protein expression level of the anti-CD19 CAR was detected
491 with an anti-CD3z antibody (Santa Cruz Biotechnology).
492
493 CAR T-cell cytotoxicity assays
494 CAR T cell cytotoxicity was determined using a FACS based assay. First,
495 NALM6 or Jeko 1 tumor cells were stained with CTV (CellTrace™ Violet, thermofisher).
496 Cells were resuspended in 10 mL PBS (5 x 10^6 cells), 5 µl CTV was added, and the
497 cells were incubated for 20 minutes at 37 °C. After incubation, 30 mL of RPMI media
498 was added and the cells incubated for an additional 5 minutes at 37 °C. The cells were
499 then gently pelleted, rinsed and resuspended in fresh ImmunoCult™-XF T Cell
500 Expansion Medium (StemCell) and 50 U/mL IL-2. Then in a round bottom 96-well plate,
501 20,000 stained tumor cells were cocultured with CAR T cells at different effector-target
502 ratios in a total volume of 200 µL for 24 hours, 48 hours and 72 hours. T cells
503 transduced with a membrane-tethered nanoluciferase reporter containing the *TCRA* 3'-
504 UTR (**Figure 4B**) were used as a negative control. The CAR T cell killing capacity was
505 measured by Flow Cytometry as diagrammed in **Figure 6–figure supplement 1B**.
506 Briefly, the 96-well plates were incubated at 4 °C for 30 minutes to terminate the killing
507 by CAR T cells. Then 2 µL of propidium iodide (1000x stock, Thermofisher) was added

508 to each column in the plate one by one and the living tumor cells were measured as

509 shown in **Figure 6–figure supplement 1B**.

510

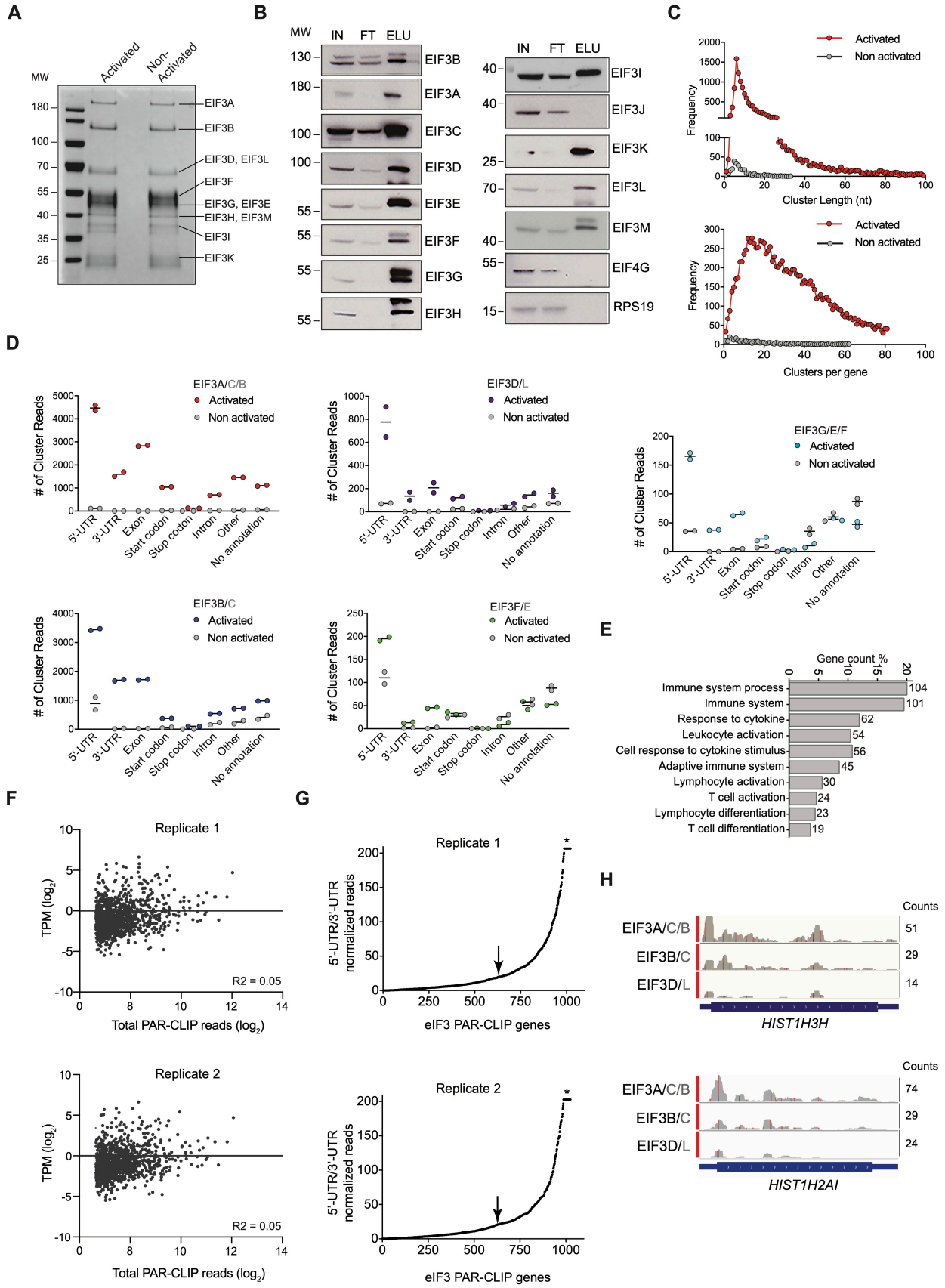
A
Activated
Non-Activated
MW
180
100
70
55
40
35
25
EIF3A
EIF3B
EIF3D, EIF3L
EIF3F
EIF3G, EIF3E
EIF3H, EIF3M
EIF3I
EIF3K
B
MW
IN FT ELU
130
180
100
100
55
55
55
55
EIF3B
EIF3A
EIF3C
EIF3D
EIF3E
EIF3F
EIF3G
EIF3H
IN FT ELU
40
40
25
70
40
55
15
EIF3I
EIF3J
EIF3K
EIF3L
EIF3M
EIF4G
RPS19
C
Activated
Non activated
Frequency
Cluster Length (nt)
Activated
Non activated
Frequency
Clusters per gene
D
EIF3A/C/B
Activated
Non activated
# of Cluster Reads
5'-UTR
3'-UTR
Exon
Start codon
Stop codon
Intron
Other
No annotation
EIF3D/L
EIF3G/E/F
EIF3B/C
EIF3F/E
E
Gene count %
Immune system process 104
Immune system 101
Response to cytokine 62
Leukocyte activation 54
Cell response to cytokine stimulus 56
Adaptive immune system 45
Lymphocyte activation 30
T cell activation 24
Lymphocyte differentiation 23
T cell differentiation 19
F
Replicate 1
TPM (log2)
R2 = 0.05
Total PAR-CLIP reads (log2)
Replicate 2
G
Replicate 1
5'-UTR/3'-UTR normalized reads
eIF3 PAR-CLIP genes
Replicate 2
H
Counts
EIF3A/C/B 51
EIF3B/C 29
EIF3D/L 14
HIST1H3H
Counts
EIF3A/C/B 74
EIF3B/C 29
EIF3D/L 24
HIST1H2AI

511

512 **Figure 1–figure supplement 1. eIF3 PAR-CLIP experiments in activated and non-**
513 **activated Jurkat cells.** (**A**) Composition of eIF3 in I+PMA activated and non-activated
514 Jurkat cells after anti-EIF3B immunoprecipitation (IP), identified by mass spectrometry.
515 Shown is an SDS polyacrylamide gel stained with Coomassie Brilliant Blue. (**B**)
516 Composition of eIF3 in activated Jurkat cells determined by western blot after anti-EIF3B
517 IP. IN: input; FT: flow-through from anti-EIF3B IP beads; ELU: elution of eIF3 from anti-
518 EIF3B IP beads. Anti-EIF4G1 and anti-RPS19 western blots confirm the stringency of
519 bead wash steps (Lee et al., 2015). (**C**) (Top) The length distribution of PAR-CLIP clusters
520 mapped to RNAs crosslinked to eIF3 in the EIF3A/C/B samples, from activated (red) and
521 non-activated (grey) Jurkat cells. (Bottom) The frequency distribution of the number of
522 eIF3 PAR-CLIP clusters mapped to RNAs in the EIF3A/C/B samples, from activated (red)
523 and non-activated (grey) Jurkat cells. In all panels, the distributions are the average of
524 both biological replicates. RNA PAR-CLIP properties observed in the EIF3A/C/B sample
525 are representative of those seen in PAR-CLIP sequence reads of RNAs crosslinked to
526 other eIF3 subunits. (**D**) Categories of RNA crosslinked to eIF3, defined by clusters and
527 divided into RNA categories, in I+PMA activated Jurkat cells and non-activated Jurkat
528 cells (grey). In all panels, RNA categories include: 5'-UTR, 5'-UTR of mRNA; 3'-UTR, 3'-
529 UTR of mRNA; CDS, protein coding region of mRNA; Start codon, beginning of mRNA
530 CDS; Stop codon, stop codon region of mRNA; Intron, regions of pre-mRNA; Other, other
531 classes of RNA; No annotation, reads that map to the human genome but that have no
532 annotation assigned. A given mRNA may give rise to clusters in different mRNA
533 categories. (**E**) Pathway enrichment categories determined using the STRING Database
534 for both biological replicates of the EIF3A/C/B PAR-CLIP libraries (mRNAs with >= 100

535 reads). Number of genes in each pathway whose mRNAs crosslinked to eIF3 is shown
536 next to each bar. Note that the categories reported by the STRING Database are not
537 disjoint sets. Panels **C** through **E** show representative results from one of two biological
538 replicates. (**F**) Scatterplot of TPM of mRNAs expressed in activated Jurkat cells (most
539 abundant isoform, see Methods) versus mRNAs identified by PAR-CLIP as crosslinked
540 to eIF3 in the EIF3A/C/B samples, with ≥ 100 total read counts. n=1,029 and 1,035 for
541 PAR-CLIP hit genes plotted for replicates 1 and 2, respectively. The R-squared goodness
542 of fit to a linear equation is shown. (**G**) mRNAs sorted by increasing value of the ratio of
543 normalized 5'-UTR reads to normalized 3'-UTR reads in the EIF3A/C/B samples. Values
544 of the ratio of 5'-UTR/3'-UTR normalized reads > 200 have been truncated to a value of
545 200 in the plot (asterisk). The arrow indicates the threshold used to create cumulative
546 plots shown in **Figure 1D**. (**H**) Examples of eIF3 crosslinking to histone mRNAs
547 *HIST1H2AI* and *HIST1H3H* in activated Jurkat cells are shown. Transcription start sites
548 were determined from the FANTOM5 Database (Noguchi et al., 2017).
549
550
551
552
553
554
555
556

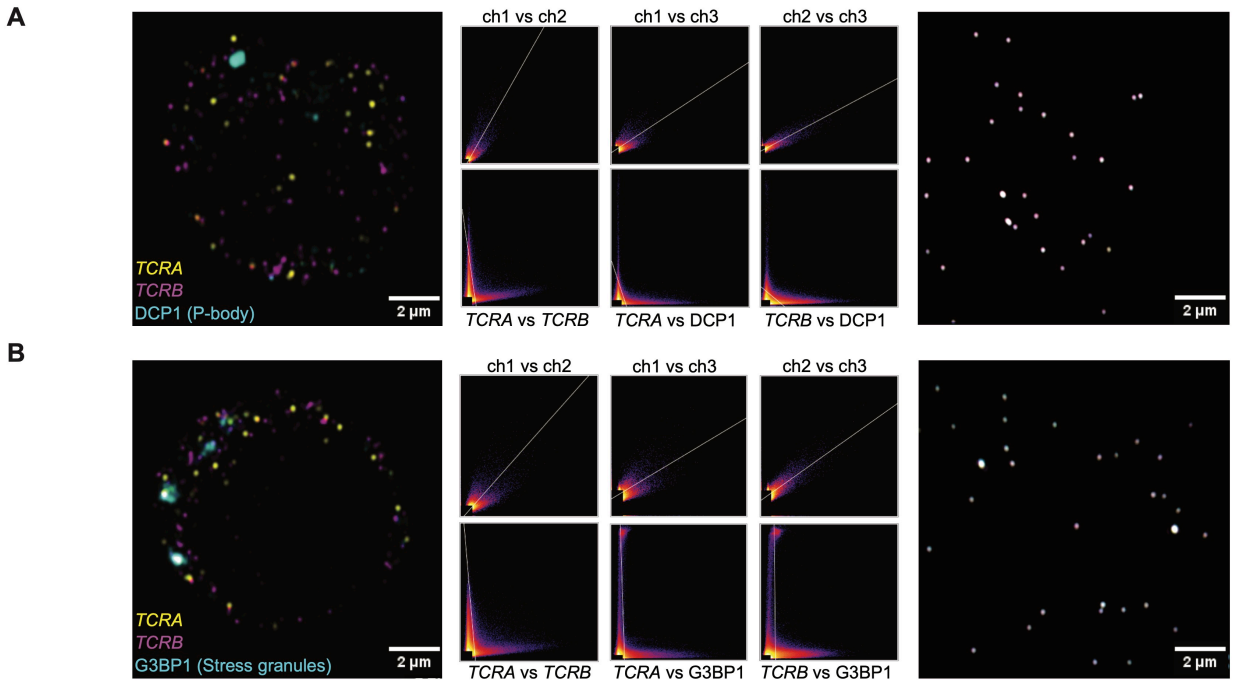

Figure 1–figure supplement 2. The *TCRA* and *TCRB* mRNAs form localized puncta in activated T cells. (**A**) (right panel) Single optical section of TetraSpeck microspheres (0.1 µm) adjacent to a Jurkat cell probed for P bodies. Scatter plots of pixel intensities in different emission channels are shown: channel 1, 670 nm; channel 2, 570 nm; channel 3, 488 nm. (left panel) Single optical section of a Jurkat cell probed for *TCRA* mRNA (channel 1), *TCRB* mRNA (channel 2), and DCP1 to mark P bodies (channel 3). (middle panels) Scatter plots showing : channel 1 vs. channel 2, channel 1 vs. channel 3, and channel 2 vs. channel 3. (**B**) (right panel) Single optical section and scatter plots for TetraSpeck microspheres as in **A**, but adjacent to a Jurkat cell probed for stress granules. (left panel) Single plane image of a Jurkat cell probed for *TCRA* mRNA (channel 1), *TCRB* mRNA (channel 2), and G3BP1 to mark stress granules (channel 3). (middle panels) Scatter plots as in **A**. Images of each cell are representative of those used in the analysis in **Figure 1F**.

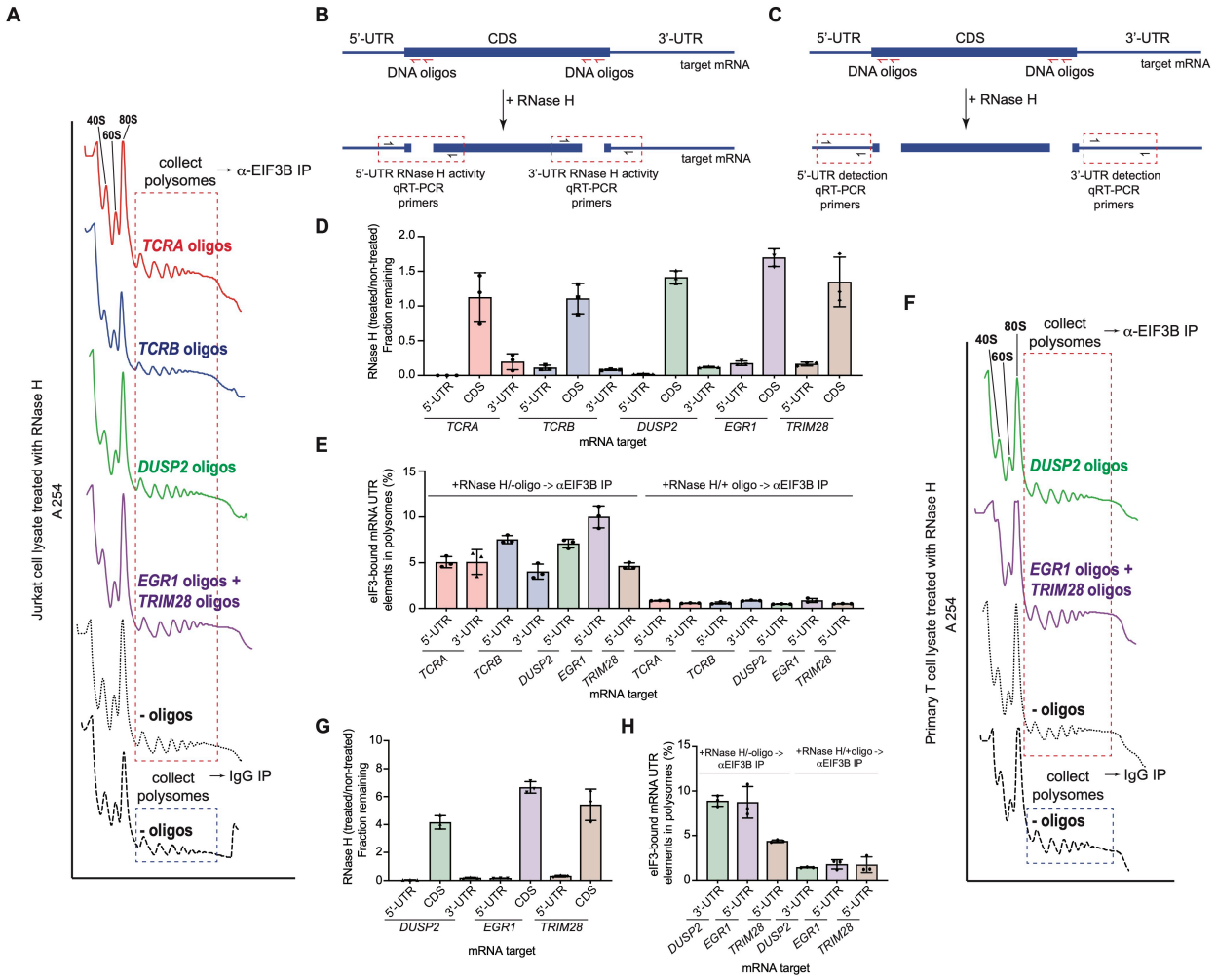

Figure 2–figure supplement 1. The *TCRA* and *TCRB* mRNAs remain bound to elongating ribosomes via eIF3 in activated T cells. (**A**) Sucrose gradient fractionation of polysomes from crosslinked Jurkat cells. Cell lysates treated with RNase H, as indicated, were fractionated on 10%-50% sucrose gradients. Shown is the absorbance at 254 nm, for one of two biological replicates. (**B**) Strategy for detecting mRNA cleavage by RNase H digestion. RT-qPCR primers were designed to span the mRNA digestion sites. (**C**) Strategy for detecting 5'-UTR or 3'-UTR mRNA fragments released by RNase H digestion. RT-qPCR primers were designed within the 5'-UTR or 3'-UTR regions. (**D**) Fraction of intact mRNA segments remaining after RNase H

581 treatment of DSP-crosslinked cell lysates from Jurkat cells, in the presence or absence
582 of mRNA-specific DNA oligos for the indicated mRNAs. The mRNAs were detected
583 using RT-qPCR oligos as illustrated in panel **B**. (**E**) Amount of eIF3-bound 5'-UTR and
584 3'-UTR regions of the mRNA co-immunoprecipitated by anti-EIF3B antibody, from
585 polysome fractions of lysate from Jurkat cells treated with RNase H, either in the
586 absence (left) or presence (right) of mRNA-targeting DNA oligos. Percentage is relative
587 to the amount of total mRNA present in the polysome fraction prior to
588 immunoprecipitation. Primers to the mRNA 5'-UTR and 3'-UTR regions, as indicated in
589 panel **C**, were used for quantification**.** (**F**) Sucrose gradient fractionation of polysomes
590 from crosslinked primary human T cells. (**G**) Fraction of intact mRNA segments
591 remaining after RNase H treatment of DSP-crosslinked cell lysates from primary T cells,
592 in the presence or absence of mRNA-specific DNA oligos for the indicated mRNAs. The
593 mRNAs were detected using RT-qPCR oligos as illustrated in panel **B**. (**H**) Amount of
594 eIF3-bound 5'-UTR and 3'-UTR regions of the mRNA co-immunoprecipitated by anti-
595 EIF3B antibody, from polysome fractions of lysate from primary human T cells treated
596 with RNase H, either in the absence (left) or presence (right) of mRNA-targeting DNA
597 oligos. Percentage is relative to mRNA present in the polysome fraction prior to
598 immunoprecipitation. Primers to the mRNA 5'-UTR and 3'-UTR regions, as indicated in
599 panel **C**, were used for quantification. All experiments were carried out in biological
600 duplicate with one technical triplicate shown (n = 3, with mean and standard deviations
601 shown). All the primary human T cell experiments were performed using samples from
602 two donors and data from one representative donor are shown.

603

604

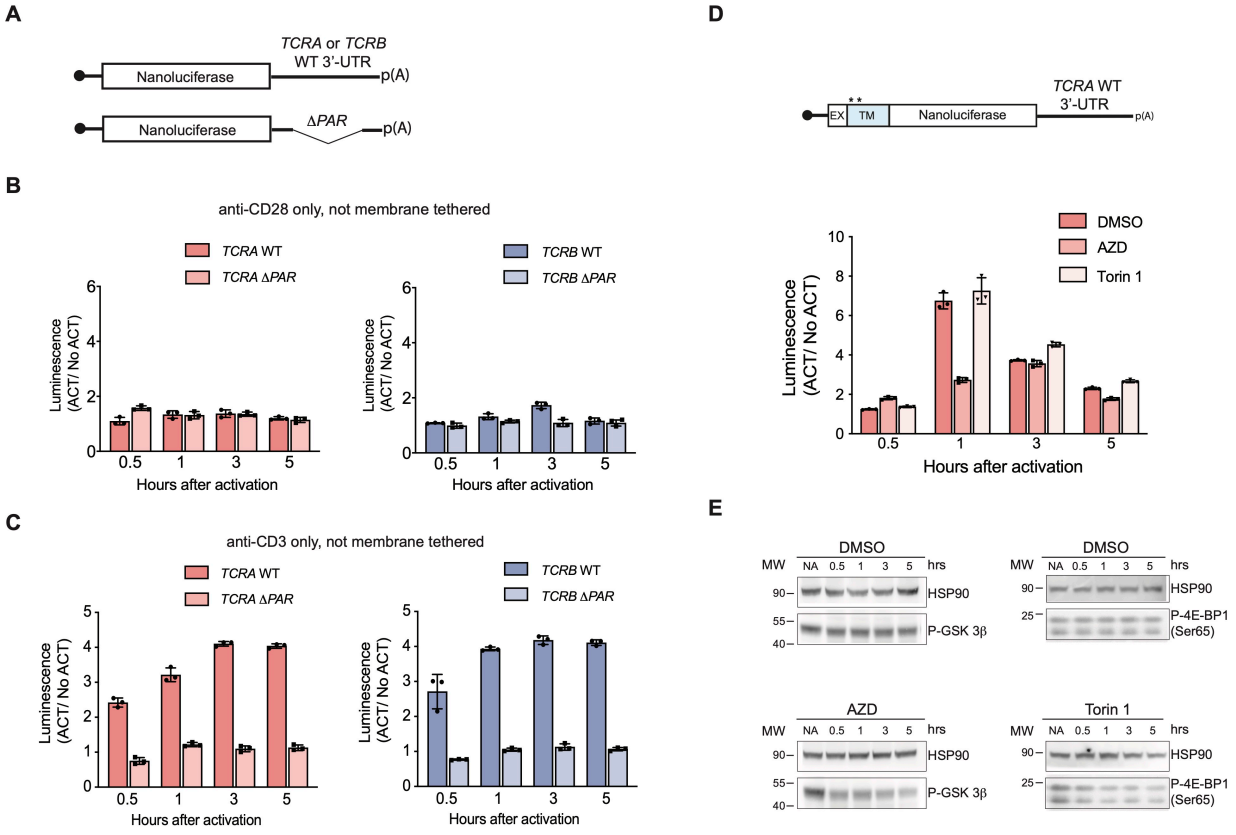

605

606 **Figure 4–figure supplement 1. Nanoluciferase reporter expression in activated T**
607 **cells.** (**A**) Schematic of nanoluciferase reporters without a transmembrane helix (not
608 membrane tethered) stably expressed in primary human T cells. The reporters carry the
609 *HBB* 5'-UTR and *TCRA, TCRB, TCRA ΔPAR,* or *TCRB ΔPAR* 3'-UTR. (**B**) Luciferase
610 activity in T cells stably expressing reporters described in **A** stimulated only with anti-
611 CD28 antibodies, relative to non-activated controls (*n* = 3, with mean and standard
612 deviations shown). (**C**) Luciferase activity in primary human T cells stably expressing
613 reporters described in **A** stimulated only with anti-CD3 antibodies, relative to non-
614 activated controls (*n* = 3, with mean and standard deviations shown). (**D**) Luciferase
615 activity in primary human T cells stably expressing membrane-tethered reporter
616 (described in the schematic above) with WT *TCRA* 3'-UTR inhibited with either

617 AZD5363(AZD) to inhibit AKT activity or Torin 1 to inhibit mTOR before activating with
618 anti-CD3/anti-CD28 antibodies, relative to non-activated controls. In panels **B**–**D**, all
619 experiments were carried out in triplicate (3 separate wells per condition), with mean and
620 standard deviations shown. (**E**) Western blot carried out to measure AKT activity in the
621 presence of AZD5363 (AZD) using an anti-Phospho-GSK-3β antibody or mTOR activity
622 in the presence of Torin 1 using an anti-Phospho-4EBP1 antibody for the samples in **D**.
623 HSP90 was used as a loading control. All the primary human T cell experiments were
624 performed using samples from two donors and data from one representative donor are
625 shown here. The data from the other donor are presented in **Figure 4F**.

626

627

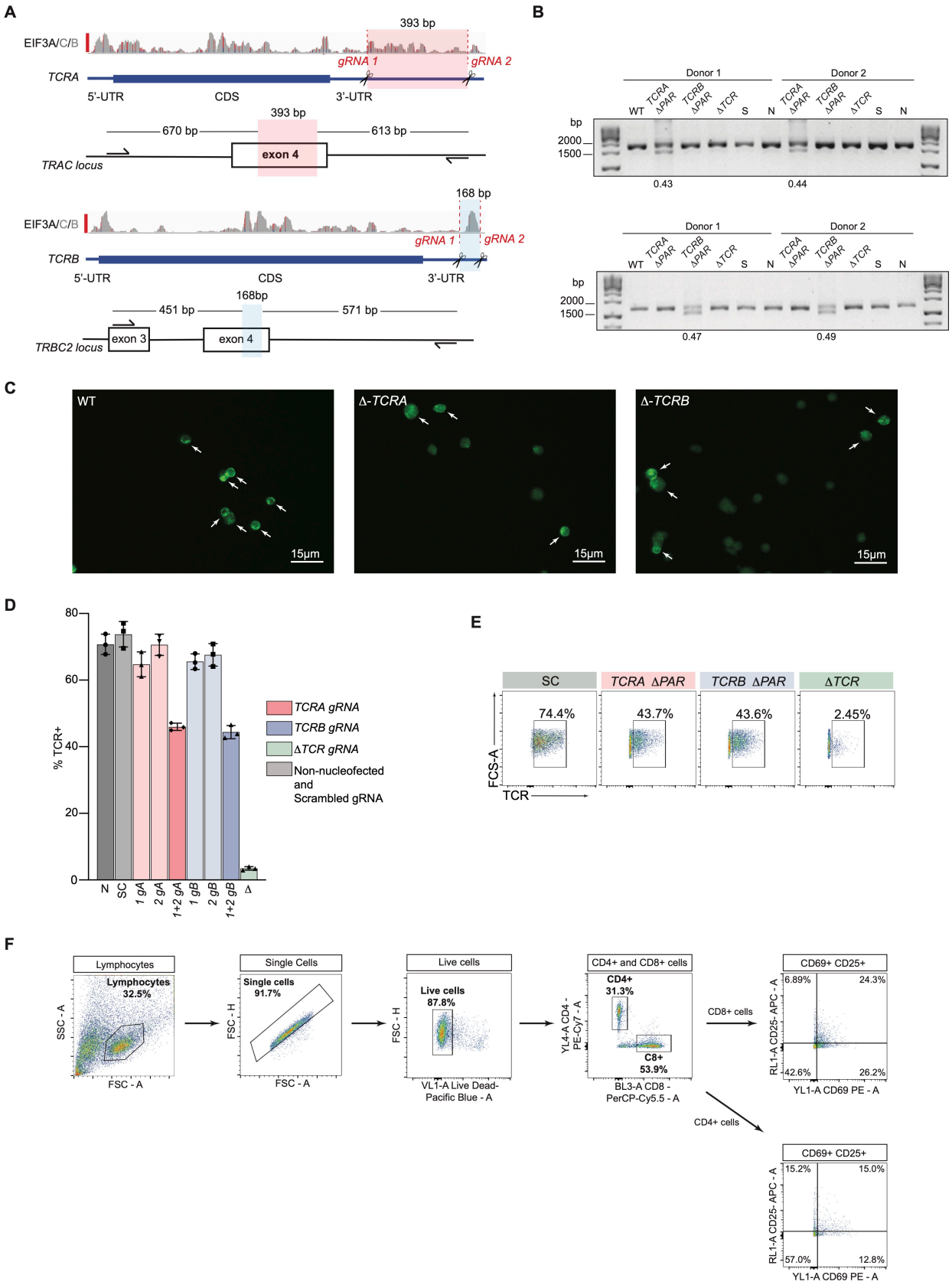
A
EIF3A/C/B
393 bp
gRNA 1
gRNA 2
TCRA
5'-UTR
CDS
3'-UTR
393 bp
670 bp
613 bp
exon 4
TRAC locus
168 bp
EIF3A/C/B
gRNA 1
gRNA 2
TCRB
5'-UTR
CDS
3'-UTR
168bp
451 bp
571 bp
exon 3
exon 4
TRBC2 locus
B
Donor 1
Donor 2
WT
TCRA ΔPAR
TCRB ΔPAR
ΔTCR
S
N
bp
2000
1500
0.43
0.44
0.47
0.49
C
WT
Δ-TCRA
Δ-TCRB
15µm
D
% TCR+
80
60
40
20
0
N
SC
1 gA
2 gA
1+2 gA
1 gB
2 gB
1+2 gB
Δ
TCRA gRNA
TCRB gRNA
ΔTCR gRNA
Non-nucleofected and Scrambled gRNA
E
SC
TCRA ΔPAR
TCRB ΔPAR
ΔTCR
74.4%
43.7%
43.6%
2.45%
FCS-A
TCR
F
Lymphocytes
Lymphocytes 32.5%
SSC - A
FSC - A
Single Cells
Single cells 91.7%
FSC - H
FSC - A
Live cells
Live cells 87.8%
FSC - H
VL1-A Live Dead-Pacific Blue - A
CD4+ and CD8+ cells
CD4+ 31.3%
C8+ 53.9%
YL4-A CD4 - PE-Cy7 - A
BL3-A CD8 - PerCP-Cy5.5 - A
CD8+ cells
CD4+ cells
CD69+ CD25+
6.89%
24.3%
42.6%
26.2%
RL1-A CD25- APC - A
YL1-A CD69 PE - A
CD69+ CD25+
15.2%
15.0%
57.0%
12.8%
RL1-A CD25- APC - A
YL1-A CD69 PE - A

628

629 **Figure 5–figure supplement 1. Generation and analysis of *TCRA* Δ*PAR* and *TCRB***
630 **Δ*PAR* primary human T cells.** (**A**) CRISPR/Cas9 RNP mediated genome editing at the
631 *TCRA* and *TCRB* genomic loci in primary human T cells. Location of gRNA sites targeting
632 the *TCRA* 3'-UTR, to generate *TCRA* Δ*PAR* cells is highlighted in red. In *TCRA*, gRNA1
633 and gRNA2 target hg38 genomic locations chr14:22,551,700 and chr14:22,552,073,
634 respectively. Location of gRNA sites targeting the *TCRB* 3'-UTR, to generate *TCRB*
635 Δ*PAR* cells is highlighted in blue. In *TCRB*, gRNA1 and gRNA2 target hg38 genomic
636 locations chr7:142,802,561 and chr7:142,802,695, respectively. (**B**) Top gel: Analysis of
637 *TCRA* 3'-UTR PAR-CLIP site deletion efficiency. Total genomic DNA extracted from WT,
638 *TCRA* Δ*PAR, TCRB* Δ*PAR* (here serving as a negative control), scrambled gRNA
639 nucleofected (S) and non-nucleofected (N) cells was analyzed by PCR to measure the
640 editing efficiency. *TCRA* Δ*PAR* cells produced a 1283 bp PCR product compared to 1676
641 bp in S, N or *TCRB* Δ*PAR* cells (See panel **A**). Bottom gel: Analysis of *TCRB* 3'-UTR
642 PAR-CLIP site deletion efficiency. Total genomic DNA extracted from WT, *TCRA* Δ*PAR*
643 (here serving as a negative control)*, TCRB* Δ*PAR*, scrambled gRNA nucleofected (S) and
644 non-nucleofected (N) cells were analyzed by PCR to measure the editing efficiency.
645 *TCRB* Δ*PAR* cells produced a 1022 bp PCR product compared to 1190 bp in S, N or
646 *TCRA* Δ*PAR* cells (See panel **A**). The percentage of alleles with PAR-CLIP site deletion,
647 quantified by imageJ. (**C**) Representative immunofluorescence images used to count
648 TCR clusters in WT, *TCRA* Δ*PAR* and *TCRB* Δ*PAR* primary human T cells. The white
649 arrows indicate the cells that were scored as having TCR clusters. (**D**) Percentage of cells
650 expressing TCR on the cell surface of activated T cells measured by flow cytometric
651 analysis. TCR expressing cells in the cell populations tested: *N*, Non-nucleofected cells;

652 SC, Scrambled gRNA; *1gA*, *TCRA* gRNA 1; *2gA*, *TCRA* gRNA 2; *1+2 gA*, *TCRA* gRNA
653 1+2 (i.e. *TCRA* Δ*PAR*); *1gB*, *TCRB* gRNA 1; *2gB*, *TCRB* gRNA 2; *1+2 gB*, *TCRB* gRNA
654 1+2 (i.e. *TCRB* Δ*PAR*); Δ*TCR*, TCR gRNA targeting the CDS of *TCRA*. (*n* = 3 replicates
655 from three separate wells, with mean and standard deviation shown.) (**E**) Representative
656 density plots showing the percentage of TCR on the cell surface in activated T cells. The
657 cell lines shown are: SC, *TCRA* Δ*PAR*, *TCRB* Δ*PAR*, Δ*TCR* (negative control). In panels
658 **D** and **E**, representative results from one of two donors are shown. (**F**) Gating strategy for
659 flow cytometric analysis of CD69 and CD25 levels. Primary human T cells were gated to
660 isolate lymphocytes, followed by isolation of single cells, then live cells. Next, cells were
661 gated to separate CD4+ and CD8+ cells expressing T cell activation markers CD69 and
662 CD25. Shown is the workflow of the FACS gating, with an example of T cells activated
663 with anti-CD3/anti-CD28 antibodies for 8 hours.

664

665

666

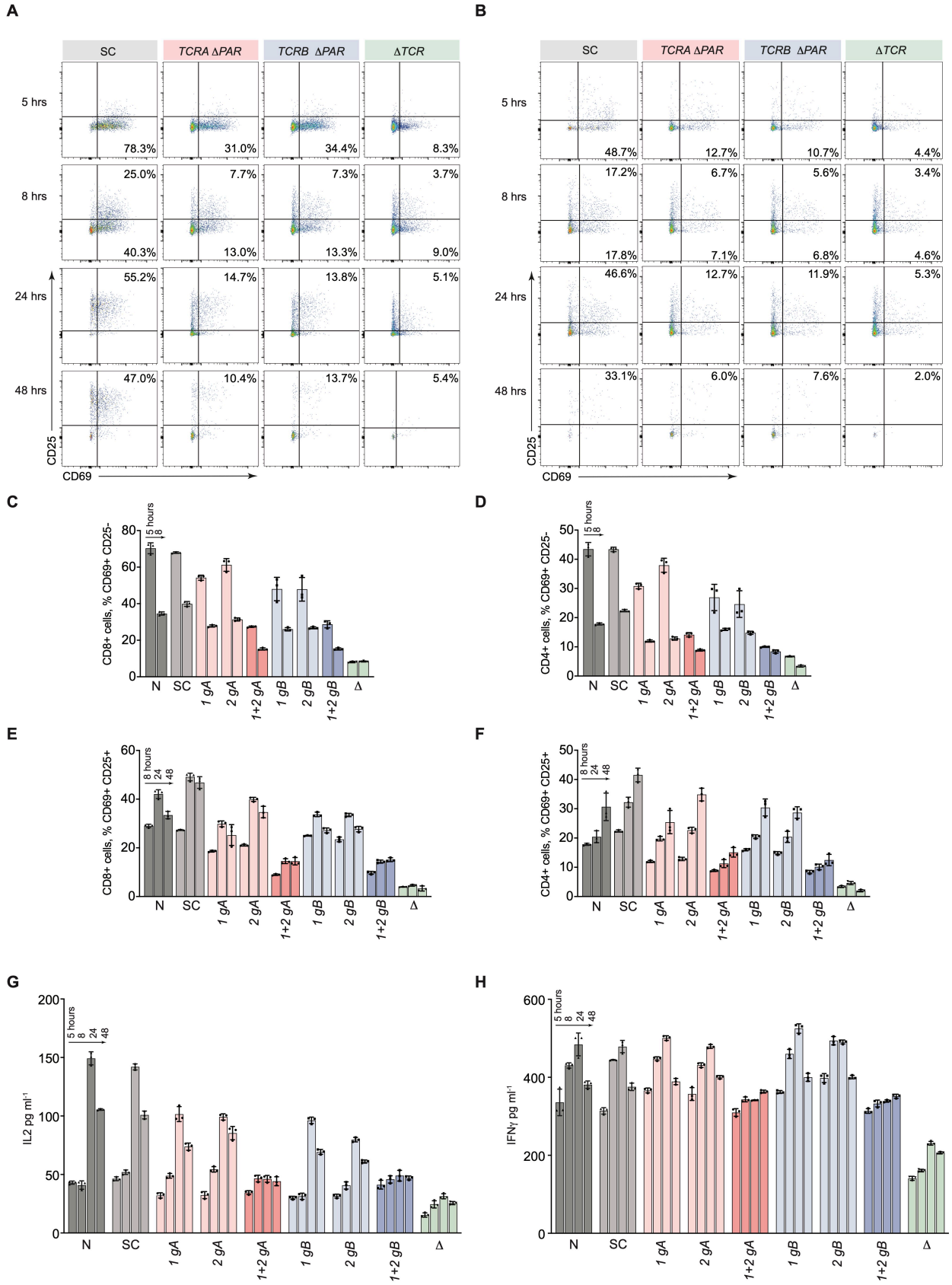
A
SC
TCRA ΔPAR
TCRB ΔPAR
ΔTCR
5 hrs
8 hrs
24 hrs
48 hrs
78.3%
31.0%
34.4%
8.3%
25.0%
7.7%
7.3%
3.7%
40.3%
13.0%
13.3%
9.0%
55.2%
14.7%
13.8%
5.1%
47.0%
10.4%
13.7%
5.4%
CD25
CD69
B
48.7%
12.7%
10.7%
4.4%
17.2%
6.7%
5.6%
3.4%
17.8%
7.1%
6.8%
4.6%
46.6%
12.7%
11.9%
5.3%
33.1%
6.0%
7.6%
2.0%
C
CD8+ cells, % CD69+ CD25-
5 hours
8
N
SC
1 gA
2 gA
1+2 gA
1 gB
2 gB
1+2 gB
Δ
D
CD4+ cells, % CD69+ CD25-
E
CD8+ cells, % CD69+ CD25+
8 hours
24
48
F
CD4+ cells, % CD69+ CD25+
G
IL2 pg ml-1
H
IFNγ pg ml-1

667

668 **Figure 5–figure supplement 2. Effects of *TCRA* Δ*PAR* and *TCRB* Δ*PAR* mutations**
669 **on different steps of T cell activation. (A** and **B)** Representative density plots showing
670 the percentage of, **A** CD8+ T cells and **B**, CD4+ T cells expressing CD69 (early activation
671 marker), CD25 (mid-activation marker) or CD69 and CD25 after activation with anti-
672 CD3/anti-CD28 antibodies at different time points, analyzed by flow cytometry. The plots
673 represent one of the two donors. The cell lines shown are SC, *TCRA* Δ*PAR*, *TCRB* Δ*PAR*
674 and Δ*TCR* (negative control). **(C** and **D)** Flow cytometric analysis quantifying the mean
675 percent of **C,** CD8+ T and **D**, CD4+ T cells that are only CD69+. **(E** and **F)** Flow cytometric
676 analysis quantifying the mean percent of **E,** CD8+ T and **F**, CD4+ T cells that are
677 CD69+CD25+. (**G** and **H**) Quantification of **G**, secreted IL-2 and **H**, secreted IFNγ, for all
678 cell populations tested, as determined by ELISA. In panels **C**–**H** cell populations tested:
679 N, Non-nucleofected cells; SC, Scrambled gRNA; *1gA*, *TCRA* gRNA 1; *2gA*, *TCRA* gRNA
680 2; *1+2 gA*, *TCRA* gRNA 1+2 (i.e. *TCRA* Δ*PAR*); *1gB*, *TCRB* gRNA 1; *2gB*, *TCRB* gRNA
681 2; *1+2 gB*, *TCRB* gRNA 1+2 (i.e. *TCRB* Δ*PAR*); *ΔTCR* gRNA targeting the CDS of *TCRA*.
682 In panels **C** through **H**, all experiments were carried out in triplicate (3 separate wells per
683 condition), with mean and standard deviations shown. Representative results from one
684 donor are shown.

685

686

687

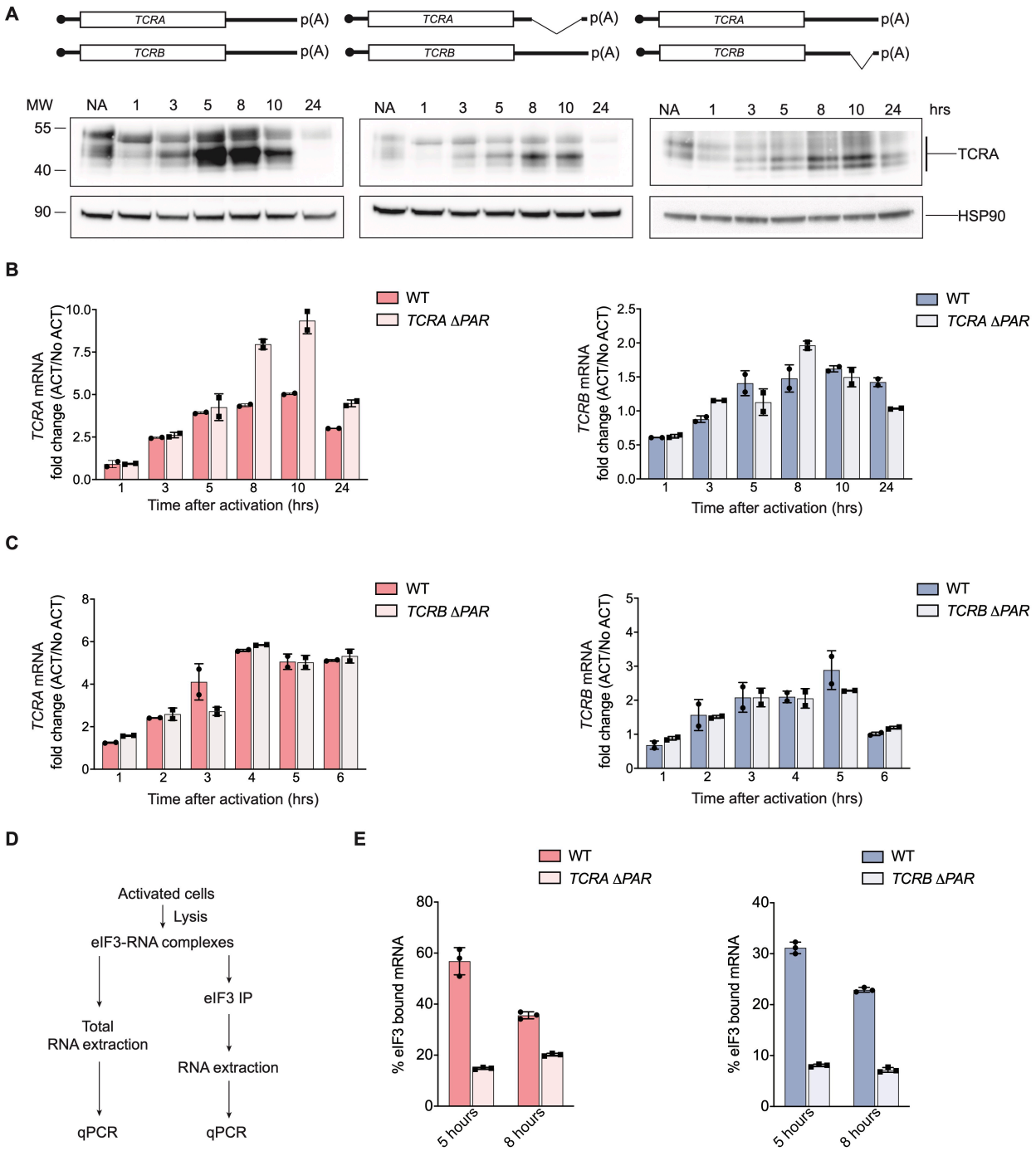

Figure 5–figure supplement 3. eIF3 binding to the *TCRA* and *TCRB* mRNA 3'-UTR elements in Jurkat cells. (**A**) Western blots of TCRA protein levels as a function of time after anti-CD3/anti-CD28 activation. Cell lines used: WT Jurkat cells, *TCRA* Δ*PAR* and *TCRB* Δ*PAR*, Jurkat cells in which the eIF3 PAR-CLIP sites in the 3'-UTRs of the *TCRA*

693 and *TCRB* mRNAs, respectively, have been deleted. Schematics of *TCRA* and *TCRB*
694 mRNAs with and without eIF3 PAR-CLIP sites are shown above. HSP90 was used as a
695 loading control. Western blots are representative of two biological replicates. (**B**) *TCRA*
696 and *TCRB* mRNA levels in WT Jurkat cells, or Jurkat cells with the *TCRA* eIF3 3'-UTR
697 PAR-CLIP site deleted, as determined by qRT-PCR at different time points after anti-
698 CD3/anti-CD28 activation. (**C**) *TCRA* and *TCRB* mRNA levels in WT Jurkat cells, or Jurkat
699 cells with the *TCRB* eIF3 3'-UTR PAR-CLIP site deleted, as determined by qRT-PCR at
700 different time points after anti-CD3/anti-CD28 activation. (**D**) Schematic of
701 immunoprecipitation of eIF3 using an anti-EIF3B antibody, followed by qRT-PCR to
702 quantify the amount of nanoluciferase mRNA bound to eIF3. (**E**) Immunoprecipitation of
703 eIF3 as shown in **D** to quantify the amount of *TCRA* or *TCRB* mRNA bound to eIF3 in
704 Jurkat cells after activation with anti-CD3/anti-CD28 antibodies for 5 hours (left) and 8
705 hours (right). The percent mRNA bound to anti-EIF3B beads is calculated relative to total
706 mRNA isolated from the cells. In panels **B**–**E**, all experiments were carried out in triplicate
707 (3 separate wells per condition), with mean and standard deviations shown.
708 Representative results from one of two biological replicates are shown.

709

710

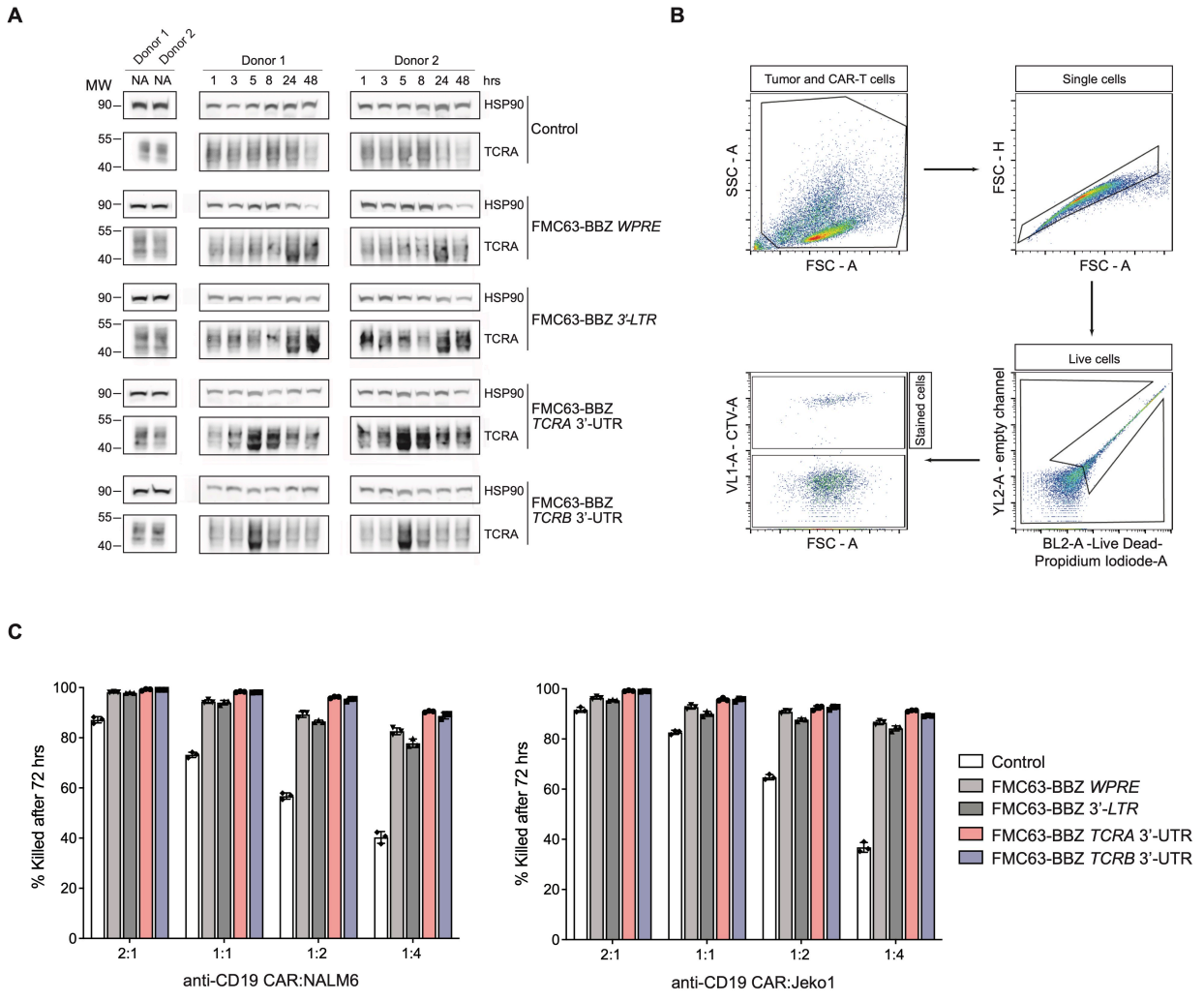

Figure 6–figure supplement 1. Effects of the *TCRA* and *TCRB* mRNA 3'-UTR elements on CAR T cell function. (**A**) Western blots measuring TCRA protein levels as a function of time in FMC63-BBZ CAR T cells after incubation with NALM6 tumor cells. Cell lines used are labeled: Control, *WPRE, 3'-LTR, TCRA* and *TCRB* 3'-UTR diagrammed in **Figure 6B**. HSP90 was used as a loading control. (**B**) Gating strategy for flow cytometric analysis to detect live tumor cells after incubation with CAR T cells. This includes: (1) both CAR T and tumor cell gating, (2) isolating single cells, (3) isolating live cells based on propidium iodide staining and (4) separating cell trace violet (CTV) stained vs non-stained cells to isolate live tumor cells. (**C**) Cytotoxic activity of FMC63-BBZ CARs

721 fused to various 3'-UTRs described in **Figure 6B** after incubating with NALM6 or Jeko1
722 tumor cell lines for 72 hours. Representative results for one of two donors are shown (*n*
723 = 3 separate wells, with mean and standard deviations shown).

724

725

726

727

728 **Supplementary Files**

729

730 **Supplementary File 1. (Separate file) Subunits in eIF3 crosslinked to RNA in**
731 **activated Jurkat cells.** Lists the eIF3 subunits, percent sequence coverage and number
732 of identified peptides.

733

734 **Supplementary File 2. (Separate file) PARpipe statistics for eIF3 PAR-CLIP**
735 **samples.** Samples are indexed in the first tab, including both biological replicates for
736 activated and non-activated Jurkat cells. Statistics are given for each library at the read,
737 cluster and group level.

738

739 **Supplementary File 3. (Separate file) PAR-CLIP mapping to individual genes for**
740 **each eIF3 PAR-CLIP sample.** Samples are indexed in the first tab, including both
741 biological replicates for activated and non-activated Jurkat cells. First lists the gene name
742 and number of clusters identified. The statistics also include: Sum, sum of that statistic
743 over all sites for that gene; Med, median of that statistic for all sites for that gene;
744 ReadCount, total reads mapping to the gene; T2C fraction, number of reads with T-to-C
745 conversions / number of reads; ConversionSpecificity, log (number of reads with T-to-C
746 conversions / number of reads with other conversions); UniqueReads, reads collapsed to
747 single copies. Also included: 5'utr/Intron/Exon/3'utr/Start_codon/Stop_codon, number of
748 sites mapping to that annotation category; Junction, number of sites mapping to a junction

749 between categories (coding-intron, coding-3'utr, etc.); GeneType, as described in the
750 gene_type category for this gene in the .gtf file used.

751

752 **Supplementary File 4. (Separate file) Transcriptome analysis of non-activated or**
753 **activated Jurkat cells.** Each tab lists transcript name and version, gene name, type of
754 transcript, length of transcript, and mean transcripts per million, calculated from two
755 biological replicates.

756

757 **Supplementary File 5. (Separate file) Pathway enrichment analysis.** Lists for both
758 biological replicates of the EIF3A/C/B PAR-CLIP libraries are included (genes with >= 100
759 reads), along with associated transcript names, lengths in nts of the 5'-UTR, coding
760 region, and 3'-UTR, and reads normalized to the lengths of the transcript regions. Tabs
761 also include the top tissue-specific pathway enrichment categories determined using the
762 STRING Database. These list: the Gene Ontology (GO) number, GO description,
763 observed gene count, background gene count, false discovery rate, and matching
764 proteins in the network by Ensembl protein ID, and by gene name.

765

766 **Supplementary File 6. (Separate file) Reagent information for experiments.** Lists
767 include antibodies used, PCR primers, qPCR primers, gRNA targeting sequences, and
768 FISH probes, and DNA oligos for RNase H experiments.

769

770

771 **References**

772 Ascano, M., Hafner, M., Cekan, P., Gerstberger, S., and Tuschl, T. (2012). Identification
773 of RNA-protein interaction networks using PAR-CLIP. Wiley Interdiscip. Rev. RNA *3*,
774 159–177.

775 Bray, N.L., Pimentel, H., Melsted, P., and Pachter, L. (2016). Near-optimal probabilistic
776 RNA-seq quantification. Nat. Biotechnol. *34*, 525–527.

777 Call, M.E., Pyrdol, J., Wiedmann, M., and Wucherpfennig, K.W. (2002). The organizing
778 principle in the formation of the T cell receptor-CD3 complex. Cell.

779 Corcoran, D.L., Georgiev, S., Mukherjee, N., Gottwein, E., Skalsky, R.L., Keene, J.D.,
780 and Ohler, U. (2011). PARalyzer: definition of RNA binding sites from PAR-CLIP short-
781 read sequence data. Genome Biol. *12*, R79.

782 Cunningham, F., Achuthan, P., Akanni, W., Allen, J., Amode, M.R., Armean, I.M.,
783 Bennett, R., Bhai, J., Billis, K., Boddu, S., et al. (2019). Ensembl 2019. Nucleic Acids
784 Res. *47*, D745–D751.

785 Danan, C., Manickavel, S., and Hafner, M. (2016). PAR-CLIP: A Method for
786 Transcriptome-Wide Identification of RNA Binding Protein Interaction Sites. Methods
787 Mol. Biol. *1358*, 153–173.

788 Dong, D., Zheng, L., Lin, J., Zhang, B., Zhu, Y., Li, N., Xie, S., Wang, Y., Gao, N., and
789 Huang, Z. (2019). Structural basis of assembly of the human T cell receptor-CD3
790 complex. Nature *573*, 546–552.

791 Frankish, A., Diekhans, M., Ferreira, A.-M., Johnson, R., Jungreis, I., Loveland, J.,
792 Mudge, J.M., Sisu, C., Wright, J., Armstrong, J., et al. (2019). GENCODE reference
793 annotation for the human and mouse genomes. Nucleic Acids Res. *47*, D766–D773.

794 Hall, M.P., Unch, J., Binkowski, B.F., Valley, M.P., Butler, B.L., Wood, M.G., Otto, P.,
795 Zimmerman, K., Vidugiris, G., Machleidt, T., et al. (2012). Engineered luciferase
796 reporter from a deep sea shrimp utilizing a novel imidazopyrazinone substrate. ACS
797 Chem. Biol. *7*, 1848–1857.

798 June, C.H., Levine, B.L., Porter, D.L., Kalos, M.D., and Milone, M.C. (2014).
799 Compositions for treatment of cancer.

800 Kalos, M., Levine, B.L., Porter, D.L., Katz, S., Grupp, S.A., Bagg, A., and June, C.H.
801 (2011). T cells with chimeric antigen receptors have potent antitumor effects and can
802 establish memory in patients with advanced leukemia. Sci. Transl. Med. *3*, 95ra73.

803 Kochenderfer, J.N., Feldman, S.A., Zhao, Y., Xu, H., Black, M.A., Morgan, R.A., Wilson,
804 W.H., and Rosenberg, S.A. (2009). Construction and preclinical evaluation of an anti-
805 CD19 chimeric antigen receptor. J. Immunother. *32*, 689–702.

806 Lee, A.S.Y., Kranzusch, P.J., and Cate, J.H.D. (2015). eIF3 targets cell-proliferation
807 messenger RNAs for translational activation or repression. Nature *522*, 111–114.

808 Martin, M. (2011). Cutadapt removes adapter sequences from high-throughput
809 sequencing reads. EMBnet.journal *17*, 10–12.

810 Milone, M.C., Fish, J.D., Carpenito, C., Carroll, R.G., Binder, G.K., Teachey, D.,

811 Samanta, M., Lakhal, M., Gloss, B., Danet-Desnoyers, G., et al. (2009). Chimeric
812 receptors containing CD137 signal transduction domains mediate enhanced survival of
813 T cells and increased antileukemic efficacy in vivo. Mol. Ther. *17*, 1453–1464.

814 Mukherjee, N., Wessels, H.-H., Lebedeva, S., Sajek, M., Ghanbari, M., Garzia, A.,
815 Munteanu, A., Yusuf, D., Farazi, T., Hoell, J.I., et al. (2019). Deciphering human
816 ribonucleoprotein regulatory networks. Nucleic Acids Res. *47*, 570–581.

817 Noguchi, S., Arakawa, T., Fukuda, S., Furuno, M., Hasegawa, A., Hori, F., Ishikawa-
818 Kato, S., Kaida, K., Kaiho, A., Kanamori-Katayama, M., et al. (2017). FANTOM5 CAGE
819 profiles of human and mouse samples. Sci Data *4*, 170112.

820 Parslow, A., Cardona, A., and Bryson-Richardson, R.J. (2014). Sample drift correction
821 following 4D confocal time-lapse imaging. J. Vis. Exp.

822 Roth, T.L., Puig-Saus, C., Yu, R., Shifrut, E., Carnevale, J., Li, P.J., Hiatt, J., Saco, J.,
823 Krystofinski, P., Li, H., et al. (2018). Reprogramming human T cell function and
824 specificity with non-viral genome targeting. Nature *559*, 405–409.

825 Schumann, K., Lin, S., Boyer, E., Simeonov, D.R., Subramaniam, M., Gate, R.E.,
826 Haliburton, G.E., Ye, C.J., Bluestone, J.A., Doudna, J.A., et al. (2015). Generation of
827 knock-in primary human T cells using Cas9 ribonucleoproteins. Proc. Natl. Acad. Sci. U.
828 S. A. *112*, 10437–10442.

829 Szklarczyk, D., Gable, A.L., Lyon, D., Junge, A., Wyder, S., Huerta-Cepas, J.,
830 Simonovic, M., Doncheva, N.T., Morris, J.H., Bork, P., et al. (2019). STRING v11:
831 protein-protein association networks with increased coverage, supporting functional

832 discovery in genome-wide experimental datasets. Nucleic Acids Res. *47*, D607–D613.

833 Voon, D.C., Subrata, L.S., Baltic, S., Leu, M.P., Whiteway, J.M., Wong, A., Knight, S.A.,
834 Christiansen, F.T., and Daly, J.M. (2005). Use of mRNA- and protein-destabilizing
835 elements to develop a highly responsive reporter system. Nucleic Acids Res. *33*, e27.

836 Wickham, H., Chang, W., and Others (2016). ggplot2: Create elegant data
837 visualisations using the grammar of graphics. R Package Version *2*.

838